Preparation of hybrids of wood sawdust with 3-aminopropyl-triethoxysilane. Application as an adsorbent to remove Reactive Blue 4 dye from wastewater effluents

Roberta A. Teixeira[1], Eder C. Lima*[2,3,4], Antônio D. Benetti[1], Pascal S. Thue[3], Mariene R. Cunha[4], Nilton F.G.M. Cimirro[4], Farooq Sher[5], Mohammad Hadi Dehghani[6,7], Glaydson S. dos Reis[8], Guilherme L. Dotto[9]

[1-]Graduate Program in Water Resources and Environmental Sanitation, Hydraulic Research Institute (IPH), Federal University of Rio Grande do Sul (UFRGS), Porto Alegre, RS, Brazil

[2-] Institute of Chemistry, Federal University of Rio Grande do Sul (UFRGS), Av. Bento Goncalves 9500, Porto Alegre, RS, Postal Box, 15003, ZIP 91501-970, Brazil

[3-] Graduate program in Science of Materials (PGCIMAT). Institute of Chemistry, Federal University of Rio Grande do Sul (UFRGS), Av. Bento Gonçalves 9500, Porto Alegre, RS, ZIP 91501-970, Brazil.

[4-] Graduate program in Mine, Metallurgical, and Materials Engineering (PPGE3M). School of Engineering, Federal University of Rio Grande do Sul (UFRGS), Av. Bento Gonçalves 9500, Porto Alegre, RS, Brazil

5- School of Mechanical, Aerospace and Automotive Engineering, Faculty of Engineering, Environment and Computing, Coventry University, Coventry CV1 5FB, UK

[6-] Department of Environmental Health Engineering, School of Public Health, Tehran University of Medical Sciences, Tehran, Iran

[7-] Institute for Environmental Research, Center for Solid Waste Research, Tehran University of Medical Sciences, Tehran, Iran

[8-] Department of Forest Biomaterials and Technology, Biomass Technology Centre, Swedish University of Agricultural Sciences, SE-901 83 Umeå, Sweden

[9-] Chemical Engineering Department, Federal University of Santa Maria (UFSM), Santa Maria, RS, Brazil

***E.C. Lima-** profederlima@gmail.com or eder.lima@ufrgs.br phone: + 55 51 3308 7175; FAX +55 51 3308 7304

Abstract

Background: Biomass-based materials present low sorption capacity. In order to overcome this disadvantage, chemical modification of these materials is required. Methods: Hybrids of biomass-based materials were obtained by reacting (25%-200% weight) 3-aminopropyl-triethoxysilane (APTES) with the biomass Ayous wood sawdust (AW), obtaining the hybrid materials AW@APTES-0.25, AW@APTES-0.50, AW@APTES-1.0, AW@APTES-1.5, and AW@APTES-2.0, that were characterized by hydrophobic/hydrophilic balance, CHN elemental analysis, surface area, TGA, FTIR, and pH_{pzc}. Significant Findings: For screening purposes, the five materials were tested as adsorbents to remove reactive blue 4 (RB-4) from water. The results showed that AW@APTES-0.5 attained the maximum removal of RB-4. The kinetics and equilibrium data were suitably fitted by the nonlinear General-order kinetic (GO) and Liu equilibrium adsorption models. The maximum amount adsorbed of RB-4 dye was 415.1 mg g^{-1} using AW@APTES-0.5 (50°C). An increase in the Q_{max} value of AW@APTES-0.5 concerning unmodified AW attained up to 21.6 times. The $\Delta G°$ and $\Delta H°$ indicated that the adsorption processes of RB-4 onto adsorbents are endothermic and spontaneous, and the magnitude of enthalpy of adsorption (25.10 kJ mol^{-1}) is compatible with the electrostatic attraction mechanism. The adsorbents' applicability for treating simulated dye effluents showed an excellent efficiency attaining 98.66% removal of the effluent.

***Keywords*:** textile effluents, biomass-based hybrid materials, thermodynamics adsorption, adsorption mechanism; nonlinear fitting.

1 Introduction

The global pigments and dyes market was valuated at 33.2 billion American dollars in 2019 [1]. Manufactures of dyes and pigments are concerned about the toxicity of these dyes, and they are actively venturing into enhancing the methods for removing dyes freed to the environment during the manufacturing process [1-3]. There is a current increasing demand for dyes for diverse industries such as textile, paints and coatings, plastics, constructions [1]. Besides the production of dyes and pigments, several industries are also responsible for considerable amounts of dyes released to the environment [1], which them the textile industry is the primary industrial sector that consumes about $^{2}/_{3}$ of all dyes that are commercialized worldwide [1].

Considering all dyes and pigments sold in 2019 [1], the Reactive Dyes has a share of 55.7% [1]. This dyes class comprises highly colored organic compounds that have primary application in tinting textiles [1]. Reactive dyes can form a covalent bond with the cotton fiber [1,4], giving them the feature of having difficulty fading and a bright shade ranges [1,4]. Although reactive dyes are primarily employed for dying textiles, 15-50% of them are left hydrolyzed in the water-baths during the dying process [5]. Therefore, high volumes of wastewater containing reactive dyes are generated, and they require further treatment before being liberated to water bodies [2,3,6-8].

Reactive Blue 4 dye (RB-4) is primarily employed in the Brazilian textiles industries [9]. RB-4 is used for dying cotton, viscose, wool, silk, and nylon. More than 50 manufacturers commercialize this dye with different trade names [9]. Based on that, it is relevant to remove RB-4 dye from aqueous effluents.

The removal of dyes from the aqueous environment is imperative because they are toxic and can cause carcinogenicity and mutagenicity [10-13]. Wastewater containing dyes are usually treated by biodegradation [14,15], coagulation-flocculation [15], the advanced

oxidative process [16], and adsorption [17-21].

The most employed method for treating wastewater containing dyes is the adsorption procedure [22,23] because of its low initial value for implementation, easy operation, a decrease in the dye's availability after the adsorption, remarkable decrease in the volume of effluent after treatment, and the possibility of the regeneration of the adsorbent after use [24,25].

Lignocellulosic wastes have been reported as adsorbents for removing dyes from wastewaters [3,26]. Although their spread is used as biosorbents, the adsorption capacities of agricultural residues are low compared with other adsorbents [6,7,24,25] because of their low surface area and the difficulty of being used in the column due to low mechanical resistance [6,7,24,25]. The chemical modification of biomass-forming hybrids and composites is a good alternative for producing adsorbents with higher adsorption capacities over unmodified lignocellulosic materials [6,7,24,25].

The 3-aminopropyl-triethoxysilane (APTES) is an organic-silane compound used for coupling with oxygen atoms present on silica, alumina, zirconia, TiO_2, and others, forming a terminal aminate group on the surface of the inorganic material [24-33]. Although it is well known that the chemical modification of inorganic materials with APTES [24-32], recently, has been reported the formation of hybrids/composite materials with biomass-based materials [7,24,25,31-36]. In this context, it is vital to produce new APTES hybrid materials with plant biomass and compare its increment in performance for removing Reactive Dyes from aqueous effluents concerning unmodified biomass.

In the present research, we proposed the chemical modification of sawdust of Ayous wood with APTES. Preliminary experiments showed that AW@APTES-0.5 is the best adsorbent for the removal of RB-4 dye from aqueous effluents. This work aimed to show that AW@APTES-0.5 material increased the maximum sorption capacity of AW biomass up to 21.6 times. This remarkable characteristic allows that the proposed adsorbent would be able to be used in actual

wastewater treatments. Besides that, the procedure for preparing the hybrid material was carried out in a single step, being an advantage when compared with adsorbents that require multiple steps for being obtained [37,38]. This research allies the need to remove reactive dyes from aqueous effluents, with a hybrid biomass-based material prepared in a single step, obtaining excellent removals from wastewater containing a complex sample matrix.

2 Materials and Methods

2.1 Reactants and solutions.

Deionized water (Permution) was used to prepare the solutions. The Reactive Blue 4 dye (RB-4; C.I. 61205) (see Fig. S1) was Merck's furnished at 95% purity. Merck furnished ethanol, 3-aminopropyl-triethoxysilane (APTES, 98%), and ammonium hydroxide (28-30% weight). The medium's acidity was adjusted using 0.1 mol L^{-1} of HCl and NaOH (Neon).

2.2 Hybrid of Ayous@APTES

Ayous sawdust was obtained from Cameroon's sawmill industries, as earlier reported [39].

Hybrid adsorbents of Ayous sawdust (AW) and APTES were synthesized using NH_4OH as a catalyst for the hydrolysis and polycondensation of APTES [7,24]. Typically, 10 g of AW was slurried in 100 mL of ethanol, and subsequently, it was added 250 µL of NH_4OH and 2.5 g of APTES. The reactional mixture was magnetically agitated at 80°C for 24 h, which allows the formation of AW@APTES hybrids using a single step [7,24] (Fig 1). Furtherly, the hybrid material was dried overnight at 75°C in a conventional furnace. The obtained hybrid was named AW@APTES-0.25. Similarly, the AW@APTES-0.50, AW@APTES-1.0, AW@APTES-1.5, and AW@APTES-2.0 were synthesized, using 10 g of AW and 5, 10, 15, and 20 g of APTES,

respectively.

Insert Fig 1

2.3 Characterization of the hybrid materials

Isotherms of adsorption and desorption of nitrogen were performed to study samples' textural characteristics using a volumetric analyzer furnished by Micromeritics Instrument (TriStar II 3020). The determination of surface area was calculated using the BET multipoint method, [40], and the pore diameter was attained using the BJHmethod [41] and DFT Method [42].

Elemental analysis (C H N/O) was carried out utilizing an Agilent elemental analyzer [43].

The functional groups present on surfaces of the samples were studied using a Fourier Transform Infra-Red (FTIR) spectrometer (Bruker, model alpha) in the range 4000–400 cm^{-1} [44].

The pH_{pzc} and hydrophobicity index (HI) of the carbon materials were obtained as described elsewhere [45,46].

The thermal stability of the AW and AW@APTES-0.5 were made by TGA analysis (TA model SDT Q600) using a heating program of 20° to 800 °C (10°C min^{-1}) under a nitrogen stream, and from 800° to 1000°C, under air gas [43,47].

2.4 Batch-contact adsorption experiments

An aliquot of 20.00 mL of RB-4 (see Fig S1) solution with the initial concentration variating from 10.0 to 1400.0 mg L^{-1} was added to 50.0 mL flat- Falcon tubes with 30.0 mg of AW and AW@APTES-X (x=0.25; 0.50; 1.0; 1.5; 2.0) at pH ranging 2.0-10.0. The Falcon tubes

were capped and disposed of horizontally inside a thermostatic reciprocating agitator (Oxy 350, São Leopoldo, Brazil). The slurries were shaken at different time intervals between 3 and 480 min at 10° to 50°C with a shaking speed of 120 strikes by minutes [47,48]. Subsequently, the solid phase was separated from the liquid phase by centrifugation. When necessary, aliquots of 1-10 ml of the liquid phase were diluted to 1.0-25.0 mL in calibrated volumetric flasks using the blank solution. The dye's unadsorbed after the adsorption process was measured using the T90+ PG Instruments spectrophotometer at a maximum absorption wavelength of 594.0 nm.

The sorption capacity (Eq 1) and the percentage of RB-4 removed (Eq 2) are given below:

$$q=\frac{(C_o-C_f)}{m}.V \tag{1}$$

$$\%Removal=100.\frac{(C_o-C_f)}{C_o} \tag{2}$$

q is the sorption capacity of RB-4 adsorbed by the adsorbent (mg g^{-1}). C_o is the initial RB-4 solution concentration in contact with the solid adsorbent (mg L^{-1}). C_f is the final RB-4 concentration after adsorption (mg L^{-1}). m is the mass of adsorbent (g). V is the aliquot of the dye solution (L) introduced in the flask.

The study of the influence of the initial pH of RB-4 was performed at 25°C, using an initial concentration of 300 mg L^{-1} of dye solution, a time of contact between the adsorbent and adsorbates of 2 h, an adsorbent dosage of 1.5 g L^{-1}, and pH ranging from 2.0 to 10.0.

The preliminary experiments were carried out to ensure reproducibility, reliability, and accuracy of the experimental data. The relative standard deviations of all measurements were below 4% [49]. Blanks were run in parallel and corrected when necessary [50].

The solutions of RB-4 were stored in glass bottles, which were cleaned, rinsing with deionized water, drying, and storing them in a suitable cabinet [51].

Standard RB-4 solutions (1.0-80.0 mg L^{-1}) were used for calibration in parallel with a blank. The linear analytical calibration curve was performed on the UV-Win software of the T90+ PG Instruments spectrophotometer. The detection limits of RB-4 were 0.21 mg L^{-1}, with a signal/noise ratio of 3 [52].

A 50.0 mg L^{-1} of standard RB-4 solutions was used as quality control after every ten measurements to ensure the analytes measurements' accuracy [50].

The kinetic and equilibrium data's fitness was done using nonlinear methods, which were evaluated using the Simplex method and the Levenberg–Marquardt algorithm using the fitting facilities of the Microcal Origin 2018 software [53]. The suitableness of the kinetic and equilibrium models was evaluated using the residual sum of squares (*RSS*), the determination coefficient (R^2), the adjusted determination coefficient (R^2_{adj}), the standard deviation of residues (*SD*), and also the Bayesian Information Criterion (*BIC*) [54]. Equations 3 to 7 are the mathematical expressions for respective *RSS*, R^2, R^2_{adj}, *SD, and BIC*.

$$RSS = \sum_{i}^{n} \left(q_{i,\,exp} - q_{i,\,model} \right)^2 \tag{3}$$

$$R^2 = \left(\frac{\sum_{i}^{n} \left(q_{i,exp} - \bar{q}_{exp} \right)^2 - \sum_{i}^{n} \left(q_{i,\,exp} - q_{i,\,model} \right)^2}{\sum_{i}^{n} \left(q_{i,exp} - \bar{q}_{exp} \right)^2} \right) \tag{4}$$

$$R^2_{adj} = 1 - \left(1 - R^2 \right) . \left(\frac{n-1}{n-p-1} \right) \tag{5}$$

$$SD = \sqrt{\left(\frac{1}{n-p} \right) . \sum_{i}^{n} \left(q_{i,\,exp} - q_{i,\,model} \right)^2} \tag{6}$$

$$BIC = \mathrm{nLn}\left(\frac{RSS}{n} \right) + pLn(n) \tag{7}$$

In the above equations, $q_{i,\,model}$ is individual theoretical q value predicted by the model; $q_{i,\,exp}$ is individual experimental q value; $\bar{q}_{exp}$ is the average of all experimental q values measured; n is the number of experiments; p is the number of parameters in the fitting model.

It will be presented the values of R^2_{adj}, SD, and BIC to compare different models of kinetics and equilibrium presented in this work. The best-fitted model would present R^2_{adj} closer to 1.000, lower values of SD, and BIC values. The kinetic and equilibrium model could not merely be chosen based on the values of R^2 [53,54] when these models present a different number of parameters. Therefore, it is necessary to check if the improvements of the R^2 values are due to the increase of a number of the parameters [53,54] or if, physically, the model with more parameters explains better the process that is taking place [53,54].

However, the difference in BIC values between models could be conclusive if the difference of BIC values ≤ 2.0, there is no significant difference between the two models [54]. When BIC values' difference is within 2-6, there is a positive perspective that the model with lower BIC is the most suitable [54]. For variations of BIC values from 6-10, there is a strong possibility of the model with a lower BIC value be the best model to be fitted [54]. However, if the difference of BIC values ≥ 10.0, it can be predicted with accuracy that the model with a lower value of BIC is the model better fitted [54].

2.5. Adsorption kinetics and equilibrium models

The kinetic adsorption data were evaluated using three models: pseudo-first-order, pseudo-second-order, and General-order kinetic models [53].

The equilibrium adsorption data were evaluated using isotherm models of Langmuir, Freundlich, and Liu [53] (see Supplementary Material).

2.6 Thermodynamics of adsorption

Thermodynamic studies for the RB-4 adsorption onto adsorbents were performed at a

temperature ranging from 10ºC to 50°C (283 to 323K).

The Gibb's free energy change (ΔG^{Θ}, kJ mol^{-1}), enthalpy change (ΔH^{Θ}, kJ mol^{-1}), and entropy change (ΔS^{Θ}, J mol^{-1}K^{-1}) were evaluated with the aid of Equations 8-12, respectively [55-57].

$$\Delta G^{\ominus} = \Delta H^{\ominus} - T\Delta S^{\ominus} \quad (8)$$

$$\Delta G^{\ominus} = -RTLn(K_e) \quad (9)$$

$$K_e = \frac{(1000.K_g.\text{molecular weight of adsorbate. standard concentration of the adsorbate})}{\text{activity coefficient of adsorbate}} \quad (10)$$

The combination of Equations 8 and 9 leads to equation 11

$$LnK_e = \frac{\Delta S^{\ominus}}{R} - \frac{\Delta H^{\ominus}}{R} x \frac{1}{T} \quad (11)$$

R is the universal gas constant (8.314 J K^{-1} mol^{-1}); T is the absolute temperature (Kelvin); K_e is the thermodynamic equilibrium constant, calculated according to equation 10. K_e is dimensionless.

K_e is calculated by converting K_g values (Liu equilibrium constant) or K_L (Langmuir equilibrium constant), expressed in L mg^{-1} into L mol^{-1}. Firstly, the value K_g or K_L is multiplied by 1000 (mg g^{-1}), and then multiplied by the molecular weight of the adsorbate (g mol^{-1}) and by the standard concentration of the adsorbate (1 mol L^{-1}) and divided by the activity coefficient of the adsorbate (dimensionless) [55,56]. It is assumed that the solution is sufficiently diluted to consider that the activity coefficient is unitary [55,56]. Making these calculations, K_e becomes dimensionless [55,56].

Equation 11 is the linearized van´t Hoff equation [57]. On the other hand, recently, Lima et al. [57] also proposed using the nonlinear van´t Hoff equation, as presented in equation 12.

$$K_e^{\ominus} = \exp\left[\frac{\Delta S^{\ominus}}{R} - \left(\frac{\Delta H^{\ominus}}{R}\right).\frac{1}{T}\right] \quad (12)$$

2.7. Synthetic effluent

Two dye-house effluents containing five reactive dyes, one organic matter, one surfactant, and seven inorganic salts were made. The chemical compositions of the effluents are presented in Table S1 [2,3,6-8,17,27,28]. These effluents' chemical composition is compatible with industrial-textile wastewater. The purpose of using simulated effluents is to test the adsorption capacities of the adsorbents for removal of the mixture of dyes in a medium that contains high concentrations of salts, surfactant, and organic matter.

3 Results and discussion

3.1 Screening of different adsorbents for the uptake of RB-4 dye

The first screening of the six adsorbents (AW, AW@APTES-0.25, AW@APTES-0.50, AW@APTES-1.0, AW@APTES-1.5, AW@APTES-2.0) as adsorbents for removing RB-4 from the water was carried out (Fig S2). This screening study is critical to characterize the samples that will significantly affect the removal of dye. As observed, all hybrid materials AW@APTES-X (X= 0.25, 0.50, 1.0, 1.5, 2.0) presented a superior adsorption capacity than unmodified wood sawdust (AW). However, for APTES amounts higher than 0.5, the adsorbent's adsorption capacity had a slight decrease and a slight worsening of the measurements' reproducibility. This loss of sorption capacity could be assigned to the formation of oligomers of APTES that did not react with OH groups present on the lignin, cellulose, and hemicellulose groups of the AW biomass [58].

The experiments were performed initially in pH 2.0 because, in earlier works where APTES grafted on different materials [7,17,27], the amino group is protonated, forming an ammonium

group positively charged that attracts the anionic RB-4 dye [7,17,27]. This behavior is one of the achievements of using APTES grafted materials for adsorbing dyes [7,17,27] concerning unmodified AW sawdust.

For continuing this work, the AW@APTES-0.5 will be material that will be wholly characterized as adsorbent because it presents a good cost/benefit relationship.

3.2 Hydrophilicity character of the hybrid surface

A critical characteristic of an adsorbent's surface is its hydrophobic/hydrophilic characteristics for the adsorption of organic molecules [7,27,28,30,43,45-48]. The addition of aminopropyl silane to lignocellulosic materials can alter the hydrophilic characteristics. The amino group is hydrophilic; however, the propyl-silane group is hydrophobic (Table S2). Observing Table 1, AW's HI values decreased from 38.2 to 45.0% for amounts of APTES ranging from 0.25 to 1.00. It means that the addition of the amine group ($-NH_2$) that is polar corroborates this result. On the other hand, for the amount of APTES ranging from 1.5 to 2.0, HI's values increased by 119.9 to 128.7%, which means that the propyl-silane group leads to a more hydrophobic characteristic.

All the materials reported in Table S2 presented HI values ranging from 0.277 to 0.931, which means that the surface of materials can adsorb more vapor of water (mg g^{-1}) than the vapor of n-heptane [7,27,28,30,43,45-48].

The HI is a vital characteristic of a solid adsorbent because it could help understand molecules' adsorption mechanism with polar groups and hydrophobic groups such as the dyes. The adsorption mechanism using a solid adsorbent depends on the chemical nature of the sorbing specie and the adsorbent [27,29,31,43,45]. Therefore, a complete understanding of adsorption's mechanism would lead to knowing the adsorbent's chemical behavior [43, 45].

3.3 Functional groups of the adsorbents

The functional groups of AW and AW@APTES-0.5 were characterized using FTIR spectroscopy (Fig 2). Fig 2A presents the spectra from 4000 to 400 cm^{-1}, and Fig 2B presents the interval from 2000 to 400 cm^{-1}. It is observed remarkable differences in the vibrational spectra of these two materials. The band at 3429 (AW) and 3386 cm^{-1} (AW@APTES-0.5) corresponds to the stretching of the -OH group [46,47]. Also, the $-NH_2$ band of the hybrid material should be overlapped with the -OH group, this band shift of 43 cm^{-1} (3429-3386 cm^{-1}) indicates the formation of AW@APTES-0.5. AW presents two bands at 2914 and 2846 cm^{-1} that could be assigned to asymmetric and symmetric C-H stretching [6,48], and AW@APTES-0.5 presented bands at 2957 and 2914 cm^{-1} that are asymmetric C-H stretching [6,7]. Both materials presented a band at 1737 cm^{-1} that could be attributed to the C=O stretch [43,44] of carboxylic acid present in lignin. Both materials presented a band at 1631 cm^{-1} that could be assigned to aromatic rings mode [43,46]; however, the hybrid material presents a broadening at 1595 cm^{-1} of this band that could also be assigned to the overlap of aromatic bands with NH_2 bending [6]. An intense peak at 1510 cm^{-1} in the hybrid material and a small band at the AW corresponds to N-H in-plane bending for AW@APTES-0.5 and aromatic ring mode for AW material, respectively. Small bands at 1458 and 1427 in both materials are assigned to aromatic ring modes [43,44]. AW presents a band at 1386 cm^{-1}, and AW@APTES-0.5 presents a band at 1371 cm^{-1} (band shift of 15 cm^{-1}) that can be assigned to -OH bending [31,45]. AW@APTES-0.5 presents a band at 1319 cm^{-1} that is assigned to C-N stretching [6,46]. Both materials presented a band at 1260 cm^{-1} assigned to C-O stretching of the lignin's phenolic group [2,3]. AW@APTES-0.5 presents a band at 1228 cm^{-1} that is attributed to the C-N stretch [6,43]. Both materials present bands at 1160, 1110 cm^{-1} that is assigned to C-O of secondary alcohols. They

also present another band at 1055 cm^{-1}, which could be assigned to C-O stretching of primary alcohol [2,3] or Si-O-Si stretching for the hybrid material [6,46]. AW@APTES-0.5 presents a band at 897 cm^{-1} assigned to Si-O stretching [28,29]. AW material presents a band at 804 cm^{-1} corresponds to out-of-phane C-H of aromatic bending [48].

Insert Fig 2

FTIR analysis's main purpose in this research is to characterize and show that the unmodified sawdust AW presented remarkable changes when it reacted with APTES, forming the hybrid material. The results depicted in Fig 2 prove that the reactions showed in Fig 1 indeed took place. The FTIR results also show the functional groups present in both materials that could be responsible for formulating a mechanism of adsorption that will be shown in the following sections.

3.4 Determination of amount of 3-aminopropyl-silane in the AW@APTES-0.5

The first quantitative analysis of AW@APTES-0.5 and AW was performed using CHN analysis (see Table S3). According to the N contents, the AW did not present N, and AW@APTES-0.5 presented 1%. Therefore it means that at each 100 g of the hybrid sample, it would contain 1.00 g of N that was introduced through the APTES grafting on the lignin (see Fig 1). After performing a stoichiometric calculation for each mol of N, it would contain one mol of $-O_3SiC_3H_8N$ attached to the hybrid material; therefore, 1.00 g of N would contain 9.57 g of the APTES groups per 100 g of hybrid (9.57% of grafting).

Also, the TGA analysis can furnish valuable information about the grafting of APTES on AW sawdust [43,46,47]. The thermal profiles of AW@APTES-0.5 and AW are presented in Fig 3.

Insert Fig 3

The thermal profiles of AW and AW@APTES-0.5 were obtained using two different atmospheres. From room temperature up to 800°C it was used inert atmosphere (N_2 stream) and from 800° to 1000°C synthetic air was used [43,47]. This choice is made to verify the thermal stability of AW and AW@APTES-0.5 under an inert atmosphere at relatively high temperatures (800°C). Moreover, in the same run, an oxidizing atmosphere will degrade all the organic compounds generating ashes [7,43,47]. In this particular case, for the hybrid material, the difference of AW@APTES-0.5´s residual mass minus the AW´s residual mass is the amount of SiO_2 left in the hybrid material.

Furthermore, from this result, it is possible to estimate the amount of APTES groups attached to the hybrid material. Making this calculation, the net SiO_2 percentage in the hybrid material was 4.81%. Making a stoichiometric calculation of one mol of SiO_2 for one mol of -$O_3SiC_3H_8N$ attached to sawdust, the percentage of APTES grafted on hybrid material was 10.73%, whose values is not so distant from the value obtained by N elemental analysis described above (9.57%).

Besides the quantitative estimation of APTES groups grafted on the biomass, both materials' thermal behavior present similitudes. Step 1 of the TGA profile of AW@APTES-0.5 is similar to steps 1 and 2 of AW biomass. Both materials are thermally stable up to 269.0° (AW@APTES-0.5) and 254.4° (AW). These weight losses correspond to releases of moisture and interstitial waters [7,43,47]. Step 2 (AW@APTES-0.5) and step 3 (AW) corresponds to the initial degradation of cellulose and hemicellulose of the carbonaceous matrix [7,43,47] and some part of the 3-aminopropyl group attached to the silica [7]. Step 3 (AW@APTES-0.5) and step 4 (AW) are the degradations of lignin of both samples forming a carbonaceous residue up to close 800°C [7,43,47]. When air synthetic is introduced into the system, rapid degradation of all carbonaceous materials takes place, and it will form ashes. It is essential to highlight that for the hybrid material, the last step (5) increases mass, which should occur due to the

recombination of the inorganics with oxygen, forming oxides [7] (see Fig 3).

From the results of nitrogen contents in Table S3 and the difference in the residual mass at 1000° of both AW@APTES-0.5 and AW showed Fig 3, it is possible to infer that the chemical reaction proposed in Fig 1 took place.

3.5 Isotherms of adsorption and desorption of nitrogen

The isotherms of adsorption and desorption of nitrogen and the DFT and BJH pore size distribution for AW@APTES-0.5 and AW are presented in Fig 4.

Insert Fig 4

Both materials present low surface areas 1.4 (AW) and 2.4 m^2 g^{-1} (AW@APTES-0.5), low total pore volumes 0.0022 (AW) and 0.0029 g cm^{-3} (AW@APTES-0.5). The isotherm of adsorption and desorption of N_2 of both materials are type II [40]. The ratio P/P_0 0.2 corresponds to the formation of a monolayer of nitrogen adsorbed for both materials [40]. This behavior is characteristic of nonporous or macroporous materials [40]. The pore size distribution curves (Fig 4B and 4D) show that both materials present a fraction of microporous and a small fraction of mesopores.

Comparing these two materials shows that the pore-filling mechanism should not be the major factor contributing to the uptake of RB-4 using AW@APTES and AW (see Fig 1) [7,24,25]. For adsorbents with presents large porosity, one of the main adsorption mechanism is the pore-filling [2,8,17,45,46,48]. Conversely, for adsorbents with a low surface area and also involving removal of charged dyes, the mechanism of adsorption is usually governed by electrostatic attraction, hydrophobic interactions, van der Walls forces, and other physical interactions mechanisms [3,6,7,22,24-26].

3.6 pH_{pzc} and effect of initial pH on the adsorption capacity

The pH_{pzc} of AW@APTES-0.5 and AW are presented in Fig 5. The chemical modification of AW with APTES shift the pHpzc from 6.051 to 10.37. Making a simulation of values of pK_a of the proposed AW@APTES-0.5 structure using the plugins of Mavin Sketch 21.1.0 (see Fig S3), pK_a values of the amino group are ranging from 9.3-11.7; and 7.00-11.7 for terminal silanol groups. Also, the estimated isoelectric point of the structure of Fig S3 was 9.86. Based on pKa and isoelectric point values, it is reasonable that the experimental pH_{pzc} of AW@APTES-0.5 be 10.37.

Insert Fig 5

For RB-4 dye solutions at pH < 10.37, the surface of the AW@APTES-0.5 will present a positively charged surface. For pH > 10.37, the surface of AW@APTES-0.5 will be negatively charged [46].

Another important point that should be highlighted is the differences in values of pH_{pzc} for AW@APTES-0.5 and AW. The grafting of AW with APTES increases the adsorbent's basicity considerably by introducing amino groups (around 10% concerning N elemental analysis and TGA results) on the surface. This increment of N basic groups on AW@APTES-0.5 is responsible for increasing this hybrid adsorbent's sorption capacity compared to unmodified AW biomass.

Fig S4 presents the effect of the initial pH on the adsorption capacity of AW@APTES and AW for adsorption of RB-4 dye. It was observed that a higher adsorption capacity was obtained at pH 2.0 for both adsorbents. For any pH values < pH_{pzc} of the adsorbent, the superficial charge will be positive. As lower the adsorbate solution's pH, the more positively charged will be the adsorbent's surface [2,3,6-8]. Considering that RB-4 is an anionic dye that presents two sulfonic groups (see Fig S1), at pH 2.0, the electrostatic attraction of positively charged adsorbents (AW and AW@APTES-0.5) with the negatively charged RB-4 dye will take place. As the pH of the

adsorbate solution increases, the adsorption capacity decreases. This observation is characteristics of electrostatic attractions of anionic dyes at low pH values being removed by carbon-based adsorbents [2,3,6-8].

For continuing this research, the dye solution's pH was fixed at 2.0, considering that both adsorbents' maximum adsorption capacity occurred using this acidity.

3.7 Kinetics of adsorption.

The kinetics data of adsorption of RB-4 dye onto AW@APTES and AW adsorbent materials were performed using pseudo-first-order (PFO), pseudo-second-order (PSO), and general-order (GO) [53], and the data are displayed in Table S4 and Fig 6.

Insert Fig 6

Observing the graphs of Fig 6, it is clear that the kinetics data did not adequately follow the PFO. The kinetic data seems to follow PSO and GO. However, to distinguish the better model, it is necessary to analyze the data depicted in Table S4. Values of R^2_{adj}, SD, and mainly BIC values [46-48, 54] help define the better model to explain the kinetic model. The GO kinetic model presented the lower values of SD, lower BIC values, and closer to 1.00 values of R^2_{adj}. However, the ΔBIC (BIC value of model 1 – BIC value of model 2) has a conclusive establishment of a physical model [54]. For $\Delta BIC \geq 10$, the BIC model that presents the low value is statistically the best-fitted model [54]. The values of ΔBIC were > 101.1 (BIC_{PFO}-BIC_{GO}) and > 18.7 ($BIC_{PSO} - BIC_{GO}$) utilizing both adsorbents (see Table S4). Therefore, it could be stated that the kinetic data of the adsorption of RB-4 dye onto AW and AW@APTES-0.5 were most suitably fitted using the GO kinetic model [54].

As earlier reported [7,8,28,31,43,44,46-48], the constant rate k is not suitable for comparing different kinetic models because it presents different units, depending on the model (see Table

3). However, an interpolation in the nonlinear fitted curve for 50% of the saturations and 95% saturation will lead to $t_{1/2}$ and $t_{0.95}$, respectively. Disregarding the values of $t_{1/2}$ and $t_{0.95}$ for PFO, the values of $t_{1/2}$ are about 10 and 12 min for AW@APTES-0.5 and AW, respectively. The $t_{0.95}$ is a good estimative to know the time for obtaining the isotherm results [7,8,28,31,43,44,46-48]. Considering the $t_{0.95}$ for GO kinetic model, these times were about 165 (AW@APTES-0.5) and 198 min (AW). Considering that higher concentrations of RB-4 could delay a little bit more, the time for performing the isotherms of adsorption was established at 240 min (4 h) to guarantee that the system attained the adsorption equilibrium utilizing both adsorbents.

Besides the values of $t_{1/2}$ and $t_{0.95}$ help establish the time for performing the isotherms, these values indicated that the kinetics of adsorption of RB-4 onto AW@APTES-0.5 is slightly faster than AW because these differences are not remarkable. The differences in the superficial area, pore size distribution, and total pore volume are also not remarkable, but the hybrid material presents slightly better values for these textural characteristics. The effect of faster kinetics with surface area, pore volume has been previously discussed in the literature [46-48].

Also, it is relevant to highlight that performing kinetic experiments of adsorption of RB-4 dye onto AW@APTES-0.5 and AW is not possible to differentiate a relevant contribution of the chemical modification of APTES in the AW biomass. The main difference is only on the amount of dye up taken (see values of q_e in Table S4) and not on the kinetic behavior. This result allied to the studies of the influence of initial pH of RB-4 dye solution (Fig S4), and also considering the grafting of APTES on the AW surface did not alter the textural characteristics of the AW (Fig 4), these set of results leads to that the adsorption mechanism of RB-4 onto both adsorbents should follow an electrostatic attraction of the anionic dye with the positively charged adsorbent at pH 2.0 [3,6,17].

In order to explore the adsorption mechanism of RB-4 onto AW@APTES-0.5 and AW adsorbents, intraparticle diffusion curves were obtained [53]. Fig 6B and 6D show that the plot

of q_t versus $\sqrt{t}$ present three sections. The first section could be assigned to the diffusion of the dye by the film [53], which was a fast step. The second stage can be assigned to the intraparticle diffusion, and the third section is the diffusion of the RB-4 dye adsorbents through the smaller pores of the adsorbents until the equilibrium is attained [53]. From the slope of the second linear portion, it was calculated that the intraparticle diffusion rate constant (k_{id}) were 5.457 and 1.387 mg g^{-1} $min^{-0.5}$ for AW@APTES-0.5 and AW adsorbents respectively. The ratio k_{id} of AW@APTES-0.5 divided by AW was 3.93 times, which means that the adsorption kinetics onto the hybrid adsorbent would be faster than the unmodified biomass. However, one of the reasons for the hybrid adsorbent present higher k_{id} can also be attributed to the higher sorption capacity of AW@APTES-0.5 adsorbent compared to AW (unmodified biomass).

3.8 Isotherms, thermodynamics, and mechanism of interaction of adsorbent with the adsorbate

The isotherms of adsorption and desorption of RB-4 dye onto AW@APTES-0.5 and AW at temperatures ranging from 10° to 50°C were performed. The equilibrium data were fitted using the nonlinear fitting of Langmuir, Freundlich, and Liu isotherm models are presented in Table S5. Fig S5 shows the isotherms at 50°C for the adsorption of RB-4 dye onto both adsorbents.

According to the results presented in Table S5, the Liu isotherm model was better fitted by the isotherm data at temperatures ranging from 10° to 50°C, because of the lowest SD and BIC and R^2_{adj} closer to 1 were obtained for this isotherm model. The ΔBIC between Langmuir and Liu ranged from 50.23 to 55.63 for temperatures 10°-40°C and 3.390 at 50°C, using the hybrid adsorbent, and 52.85 to 104.3 for 10° to 50°C using AW biomass [54]. Although just for one temperature and one case, the ΔBIC ($BIC_{Langmuir} - BIC_{Liu}$) was not conclusive; however, there is a perspective that the Liu model would be the better isotherm model to be fitted at 50°C

concerning Langmuir isotherm, using the hybrid adsorbent [54]. For all ΔBIC ≥10 it is conclusive that the Liu model was the best-fitted model. The $BIC_{Freudlich} - BIC_{Liu}$ ranged from 62.19 to 123.5 (AW@APTES-0.5) and 90.06-124.7 (AW) for temperature from 10° to 50°C. Therefore, considering the adsorption of RB-4 onto both adsorbents, the equilibrium data were successfully fitted by the Liu model at the temperature range from 10° to 50°C.

Considering the values of Q_{max} obtained by the Liu isotherm for both adsorbents, it is observed that AW@APTES-0.5 presented values 8.8-21.6 times higher than AW. This considerable increase in the adsorption capacity is due to the possible formation of AW@APTES-0.5 depicted in Fig 1. The insertion of amino groups on the hybrid material leads to positively charged ammonium groups when the adsorbent is immersed in a solution with pH 2.0, facts that allow attracting the anionic RB-4 dye electrostatically.

Table S6 and Fig S6 [55,56] present the thermodynamic data of adsorption of RB-4 dye onto AW@APTES-0.5 and AW adsorbents.

As can be seen, the result of thermodynamic of adsorption for the adsorption of RB-4 dye onto two adsorbents, the process of adsorption was spontaneous within the range of temperatures used (283-323 K), where the value of $\Delta G^{\Theta} < 0$, the values of $\Delta H^{\Theta} > 0$, pointing that the process of adsorption was endothermic in both cases (see Fig S6) [57]. Also, the magnitude of enthalpy changes is compatible with physical adsorption [59,60]. For both cases, the ΔS° were also positive, indicating that the sorbing specie should have lost hydration water before occupying the adsorbent's active site [46,47].

Considering the data of the surface area, pore size distribution, HI, pH_{pzc} of the adsorbents, the chemical nature of the adsorbents, the studies of initial pH of the sorbing solution, the study of kinetics, and the thermodynamic results for adsorption of the anionic RB-4 dye onto AW@APTES-0.5 and AW, it is possible to state that the mechanism of interaction of the adsorbent with the adsorbate is an electrostatic attraction of the anionic RB-4 dye onto the

protonated amino groups of the adsorbent at pH 2.0 (see Fig 7).

Insert Fig 7.

The probable mechanism of interaction of the adsorbent with the adsorbate should take place in two steps. In the first step, the amino groups at pH 2.0 are protonated, forming positively charged ammonium specie. The RB-4 anionic dye is electrostatically attracted by the ammonium group (positively charged) at the second stage, forming an ion pair. This interaction mechanism should be the primary mechanism of adsorption, disregarding the transport phenomena. Other less significant mechanisms are hydrogen-bonding, π-π interaction of RB-4 rings with AW's aromatics, van der Waals interactions [43,47]. The mechanism of pore-filling should be disregarded, considering the low surface area of both adsorbents. In the AW material, where there are no 3-aminopropyl groups, the interaction mechanism is limited to hydrogen-bonding, π-π interaction of RB-4 rings with AW's aromatics, van der Waals interactions [43,47], and electrostatic attraction. For the AW material, the mechanism is still the electrostatic attraction; however, there is no amino group presence as in the hybrid material, limiting the sorption capacity compared to AW@APTES-0.5.

3.9 Simulated effluents

Two synthetic effluents were prepared to verify the performance of the AW@APTES-0.5 and AW as adsorbents for the treatment of textile wastewater effluents (see Table S1). An adsorbent with potential application in real situations should present a good removal in a medium containing several compounds [2,3,6,7,8,17,27,28]. Fig 8 presents the UV-VIS spectrum of the simulated effluents A and B before the adsorption (spectra in black) and after treatment with AW@APTES-0.5 (red spectra) and AW (blue spectra).

Insert Fig 8

For calculating the overall removal percentage, it was integrated the area under the curves [43]. Taking into account that absorbance is an additive property [43], the absorbance of each component present in the effluents is summed during the integration [43]. The percentage of removal can be calculated by the spectra area after treatment divided by the effluent area before the treatment [43]. For effluent A, the obtained overall removals were 98.66% (AW@APTES-0.5) and 10.24% (AW) (see Fig 8). For effluent B, which presents higher concentrations of the components, the obtained overall removals were 98.52% (AW@APTES-0.5) and 9.15% (AW). These results show AW@APTES-0.5 which presents a maximum adsorption capacity of 276.8 mg g^{-1} (25°C, see Table S5), has the potential for being employed as an adsorbent for the treatment of dying containing textile wastewaters. On the other hand, AW's unmodified sawdust that presents a lower maximum adsorption capacity (12.81 mg g^{-1} at 25°C) can not be used as a potential adsorbent for wastewater treatment.

Conclusion

Ayous sawdust (AW) was chemically modified with different proportions of APTES, forming AW@APTES-0.25, AW@APTES-0.50, AW@APTES-1.0, AW@APTES-1.5, and AW@APTES-2.0. In the first screening of these adsorbents for removing the Reactive Blue 4 dye (RB-4), it was shown that the AW@APTES-0.50 material is the best hybrid material for continuing the work because of its higher sorption capacity and lower variability of the results. In order to compare the differences in performance of AW@APTES-0.5, the unmodified biomass (AW) was used. Nitrogen isotherms of adsorption and desorption characterized both AW@APTES-0.50 and AW, and the results showed that both materials have low surface areas and poor porosities. This result indicated that the mechanism of pore filling should be disregarded. Using TGA (10.73%) and C H N elemental analysis (N analysis 9.57%), it was

possible to estimate the percentage of APTES grafted on AW material. The probable grafting of APTES on sawdust (see Fig 1) increased the hydrophilicity feature of AW@APTES-0.50 compared to AW and also shifted the pH_{pzc} from 6.051 (AW) to 10.37 (AW@APTES-0.50), which confer a basic characteristic to the hybrid material. Studies of the effect of the initial pH of RB-4 on the adsorption capacity of both adsorbents showed that pH 2.0 is the best acidity to obtain the maximum removal of the dye using both adsorbents. The adsorption kinetics data were better fitted to the nonlinear general order kinetic model (GO), and the equilibrium data obtained at temperatures ranging from 10° to 50°C showed that the nonlinear Liu isotherm model represented better the equilibrium of adsorption. The thermodynamics of adsorption showed that the process of adsorption was favorable ($\Delta G° < 0$), endothermic ($\Delta H° > 0$), and the magnitude of enthalpy changes is compatible with physical adsorption. Based on all the results obtained in this work, a mechanism of adsorption where the main contribution is the electrostatic attraction of the anionic dye with the positively charged adsorbent at pH 2.0 should take place. Results of treatment of simulated effluents showed that AW@APTES-0.50 is a potential adsorbent for being employed in real applications because the efficiency of removal attained up to 98.66% of a sample with a complex formulation (see Table S1).

Acknowledgments

The authors thank CNPq, CAPES, and FAPERGS for financial support and fellowships. The authors are grateful to Nanoscience and Nanotechnology Center (CNANO-UFRGS) and Microscopy and Microanalysis Center (CME-UFRGS) of the Federal University of Rio Grande do Sul (UFRGS). We are also grateful to ChemAxon for giving us an academic research license for the Marvin Sketch software, Version 21.3.0 (http://www.chemaxon.com), 2021 used for molecule physical-chemical properties.

References

[1] Global Dyes and Pigments Market Size Report, 2020-2027. Website visited on February 12th, 2021. https://www.grandviewresearch.com/industry-analysis/dyes-and-pigments-market.

[2] Puchana-Rosero, M.J., Adebayo, M.A., Lima, E.C., Machado, F.M., Thue, P.S., Vaghetti, J.C.P., Umpierres, C.S., Gutterres, M. Microwave-assisted activated carbon obtained from the sludge of tannery-treatment effluent plant for removal of leather dyes. Colloids and Surfaces A: Physicochem Eng Aspects 504 (2016) 105-115.

[3] Alencar, W.S., Lima, E.C., Royer, B., dos Santos, B.D., Calvete, T., da Silva, E.A., Alves, C.N. Application of aqai stalks as biosorbents for the removal of the dye Procion Blue MX-R from aqueous solution. Sep Sci Technol 47 (2012) 513-526.

[4] Matyjas, E., Rybicki, E. Novel reactive red dyes. Autex Res J 3 (2003) 90-95.

[5] Hessel, C., Allegre, C., Maisseu, M., Charbit, F., Moulin, P. Guidelines and legislation for dye house effluents. J Environ Manage 83 (2007) 171-180.

[6] Adebayo, M.A., Prola, L.D.T., Lima, E.C., Puchana-Rosero, M.J., Cataluña, R., Saucier, C., Umpierres, C.S., Vaghetti, J.C.P., da Silva, L.G., Ruggiero, R. Adsorption of Procion Blue MX-R dye from aqueous solutions by lignin chemically modified with aluminum and manganese. J Hazard Mater 268 (2014) 43-50.

[7] Leite, A.J.B., Lima, E.C., dos Reis, G.S., Thue, P.S., Saucier, C., Rodembusch, F.S., Dias, S.L.P., Umpierres, C.S., Dotto, G.L. Hybrid adsorbents of tannin and APTES (3-aminopropyltriethoxysilane) and their application for the highly efficient removal of acid red 1 dye from aqueous solutions. J Environ Chem Eng 5 (2017) 4307-4318.

[8] Machado, F.M., Sophia A.C., Lima, E.C., Dias S.L.P., Prola, L.D.T., Saucier, C., Jauris, I.M., Zanella, I., Fagan, S.B. Adsorption of Alizarin Red S Dye by Carbon Nanotubes-

An Experimental and Theoretical Investigation. J Phys Chem C 120 (2016) 18296−18306.

[9] Reactive Blue 4. Dye World variety. http://www.worlddyevariety.com/reactive-dyes/reactive-blue-4.html web site visited May 6th, 2021.

[10] de Lima, R.O.A., Bazo, A.P., Salvadori, D.M.F., Rech, C.M., Oliveira, D.P., Umbuzeiro, G.A. Mutagenic and carcinogenic potential of a textile azo dye processing plant effluent that impacts a drinking water source. Mutat Res Genet Toxicol Environ Mutagen 626 (2007) 53-60.

[11] Kaledin, V.I., Ilnitskaya, S.I., Ovchinnikova, L.P., Popova, N.A., Bogdanova, L.A., Morozkova, T.S. Mutagenic Activation and Carcinogenicity of Aminoazo Dyes ortho Aminoazotoluene and 3' Methyl-4- Dimethyl-amino-azobenzene in Experiments on Suckling Mice. Biophysics 59 (2014) 431–435.

[12] Alderete, B. L., da Silva, J., Godoi, R., da Silva, F.R., Taffarel, S.R., da Silva, L.P., Garcia, A.L.H., Mitteregger-Jr., H., de Amorim, H.L.N., Picada, J.N. Evaluation of toxicity and mutagenicity of a synthetic effluent containing azo dye after Advanced Oxidation Process treatment. Chemosphere 263 (2021) 128291. doi:10.1016/j.chemosphere.2020.128291.

[13] Koktürk, M., Altindag, F., Ozhan, G., Çalimli, M.H., Nas, M.S. Textile dyes Maxilon blue 5G and Reactive blue 203 induce acute toxicity and DNA damage during embryonic development of Danio rerio. Comparative Biochemistry, and Physiology, Part C 242 (2021) 108947. Doi:10.1016/j.cbpc.2020.108947.

[14] Goud, B.S., Cha, H.L., Koyyada, G., Kim, J.H. Augmented Biodegradation of Textile Azo Dye Effluents by Plant Endophytes: A Sustainable, Eco-Friendly Alternative. Curr Microbiol 77, (2020) 3240–3255.

[15] Ayed, L., El-Ksibi, I., Charef, A., El-Mzoughi, R. Hybrid coagulation-flocculation and anaerobic-aerobic biological treatment for industrial textile wastewater: a pilot case study. J Text Inst 112 (2021) 200-206.

[16] Santana, R.M.R., Charamba, L.C.V., do Nascimento, G.E., de Oliveira, J.G.C, Sales, D.C.S., Duarte, M.M.M.B., Napoleão, D.C. Degradation of Textile Dyes Employing Advanced Oxidative Processes: Kinetic, Equilibrium Modeling, and Toxicity Study of Seeds and Bacteria. Water Air Soil Pollut 230 (2019) 136. Doi:10.1007/s11270-019-4178-x.

[17] de Menezes, E.W., Lima, E.C., Royer, B., de Souza, F.E., dos Santos, B.D., Gregório, J.R., Costa, T.M.H., Gushikem, Y., Benvenutti, E.V. Ionic silica-based hybrid material containing the pyridinium group used as an adsorbent for textile dye. J Colloid Interface Sci 378 (2012) 10-20.

[18] Wu, J., Liu, J., Wen, B., Li, Y., Zhou, b., Wang, Z., Yang, S., Zhao, R. Nitrogen-rich covalent triazine frameworks for high-efficient removal of anion dyes and the synergistic adsorption of cationic dyes. Chemosphere 272 (2021) 129622. Doi: 10.1016/j.chemosphere.2021.129622.

[19] Ji, Y., Zhang, W., Yang, H., Ma, F., Xu, F. Green synthesis of poly(pyrrole methane) for enhanced adsorption of anionic and cationic dyes from aqueous solution. J. Colloid Interface Sci 590 (2021) 396-406.

[20] Reghioua, A., Barkat, D., Jawad, A.H., Abdulhameed, A.S., Khan, M.R. Synthesis of Schiff's base magnetic crosslinked chitosan-glyoxal/ZnO/Fe_3O_4 nanoparticles for enhanced adsorption of organic dye: Modeling and mechanism study. Sustainable Chem Pharm 20 (2021) 100379. Doi:10.1016/j.scp.2021.100379.

[21] Didehban, A., Zabihi, M., Faghihi, M., Akbarbandari, F., Akhtarivand, H. Design and fabrication of core-shell magnetic and non-magnetic supported carbonaceous metal-organic framework nanocomposites for adsorption of dye. J Phys Chem Solids 152 (2021) 109930. Doi:10.1016/j.jpcs.2020.109930.

[22] dos Santos, J.M.N., Pereira, C.R., Pinto, L.A.A., Frantz, T., Lima, E.C., Foletto, E.L.,

Dotto, G.L. Synthesis of a novel $CoFe_2O_4$/chitosan magnetic composite for fast adsorption of indigotine blue dye. Carbohyd Polym 217 (2019) 6-14.

[23] Abdel-Ghani, N.T., El-Chaghaby, G.A., Rawash, E.S.A., Lima, E.C. Magnetic activated carbon nanocomposite from *Nigella sativa* L. waste (MNSA) for the removal of Coomassie brilliant blue dye from aqueous solution: Statistical design of experiments for optimization of the adsorption conditions. J Adv Res 17 (2019) 55-63.

[24] Carijo, P.M., dos Reis, G.S., Lima, E.C., Dotto, G.L. Functionalization of corn stover with 3–aminopropyl-triethoxysilane to uptake Reactive Red 141 from aqueous solutions. Environ Sci Pollut Res 26 (2019) 32198–32208.

[25] Lima, V.V.C., Nora, F.B.D., Peres, E.C., Reis, G., Lima, E.C., Oliveira, M.L.S., Dotto, G.L. Synthesis and characterization of biopolymers functionalized with APTES (3–aminopropyltriethoxysilane) for the adsorption of sunset yellow dye. J Environ Chem Eng 7 (2019) 103410. Doi:10.1016/j.jece.2019.103410.

[26] Franco, D.S.P., Tanabe, E.H., Bertuol, D.A., dos Reis, G.S., Lima, E.C., Dotto, G.L. Alternative treatments to improve the potential of rice husk as an adsorbent for methylene blue. Water Sci Technol 75 (2017) 296-305.

[27] Wamba, A.G.N., Lima, E.C., Ndi, S.K., Thue, P.S., Kayem, J.G., Rodembusch, F.S., dos Reis, G.S., de Alencar, W.S. Synthesis of grafted natural pozzolan with 3-aminopropyltriethoxysilane: Preparation, characterization, and application for removal of Brilliant Green 1 and Reactive Black 5 from aqueous solutions. Environ Sci Pollut Res 24 (2017) 21807–21820.

[28] Thue, P.S., Sophia, A.C., Lima, E.C., Wamba, A.G.N., de Alencar, W.S., dos Reis, G.S., Rodembusch, F.S., Dias, S.L.P. Synthesis and characterization of a novel organic-inorganic hybrid clay adsorbent for the removal of acid red 1 and acid green 25 from aqueous solutions. J. Clean. Prod. 171 (2018) 30-44.

[29] Wamba, A.G.N., Kofa, G.P., Koungou, S.N., Thue, P.S., Lima, E.C., dos Reis, G.S., Kayem, J.G. Grafting of Amine functional group on silicate-based material as an adsorbent for water purification: A short review. J Environ Chem Engin 6 (2018) 3192-3203.

[30] Wamba, A.G.N., Ndi, S.K., Lima, E.C, Kayem, J.G., Thue, P.S., Costa, T.M.H., Quevedo, A.B., Benvenutti, E.V., Machado, F.M. Preparation, characterization of titanate nanosheet–pozzolan nanocomposite and its use as an adsorbent for removal of diclofenac from simulated hospital effluent. J Taiwan Inst Chem Eng 102 (2019) 321-329.

[31] Caicedo, D.F., dos Reis, G.S., Lima, E.C., de Brum, I.A.S., Thue, P.S., Cazacliu, B.G., Lima, D.R., dos Santos, A.H., Dotto, G.L. Efficient adsorbent based on construction and demolition wastes functionalized with 3-aminopropyltriethoxysilane (APTES) for the removal ciprofloxacin from hospital synthetic effluents. J Environ Chem Eng 8 (2020) 103875. Doi:10.1016/j.jece.2020.103875.

[32] Dogar, S., Nayab, S., Farooq, M.Q., Said, A., Kamran, R., Duran, H., Yameen, B. Utilization of Biomass Fly Ash for Improving Quality of Organic Dye-Contaminated Water. ACS Omega 5 (2020) 15850−15864.

[33] Nematidil, N., Sadeghi, M., Nezami, S., Sadeghi, H. Synthesis and characterization of Schiff-base-based chitosan-g-glutaraldehyde/NaMMTNPs-APTES for removal Pb^{2+} and Hg^{2+} ions. Carbohyd Polym 222 (2019) 114971. Doi:10.1016/j.carbpol.2019.114971.

[34] Laureano-Anzaldo, C.M. , Haro-Mares, N.B., Meza-Contreras, J.C., Robledo-Ortíz, J.R., Manríquez-González, R. Chemical modification of cellulose with zwitterion moieties used in the uptake of red Congo dye from aqueous media. Cellulose 26 (2019) 9207–9227.

[35] An, L., Si, C., Bae, J.H., Jeong, H., Kim, Y.S. One-step silanization and amination of lignin and its adsorption of Congo red and Cu(II) ions in an aqueous solution. Int J Biol

Macromol 159 (2020) 222–230.

[36] Fotsing, P.N., Bouazizi, N., Woumfo, E.D., Mofaddel, N., Derf, F.L., Vieillard, J. Investigation of chromate and nitrate removal by adsorption at the surface of an amine-modified cocoa shell adsorbent. J Environ Chem Eng 9 (2021) 104618. Doi:10.1016/j.jece.2020.104618.

[37] Bayat, A., Tati, A., Ahmadipouya, S., Haddad, S.A., Arjmand, M. Electrospun chitosan/polyvinyl alcohol nanocomposite holding polyaniline/silica hybrid nanostructures: An efficient adsorbent of dye from aqueous solutions. J Mol Liq 331 (2021) 115734. doi:10.1016/j.molliq.2021.115734.

[38] Sirajudheen, P., Karthikeyan, P., Vigneshwaran, S., Basheer, M.C., Meenakshi, S. Complex interior and surface modified alginate reinforced reduced graphene oxide-hydroxyapatite hybrids: Removal of toxic azo dyes from the aqueous solution. Int J Biol Macromol 175 (2021) 361-371.

[39] Nisar, M., Thue, P.S., Maghous, M.B., Geshev, J., Lima, E.C., Einloft, S. Polysulfone metal-activated carbon magnetic nanocomposites with enhanced CO_2 capture. RSC Adv 10 (2020) 34595. Doi: 10.1039/d0ra06805e.

[40] Thommes, M., Kaneko, K., Neimark, A.V., Olivier, J.P., Rodriguez-Reinoso, F.J., Rouquerol, K.S., Sing, W. Physisorption of gases, with special reference to the evaluation of surface area and pore size distribution (IUPAC Technical Report). Pure Appl Chem 87 (2015) 1051–1069.

[41] Haghighatju, F., Rafsanjani, H.H., Esmaeilzadeh, F. Estimation of the dimension of micropores and mesopores in single-walled carbon nanotubes using the method Horvath–Kawazoe, Saito and Foley and BJH equations. Micro & Nano Letters 12 (2017) 1-5.

[42] Jagiello, J., Thommes, M. Comparison of DFT characterization methods based on N_2, Ar, CO_2, and H_2 adsorption applied to carbons with various pore size distributions. Carbon 42

(2004) 1227-1232.

[43] Thue, P.S., Umpierres, C.S., Lima, E.C., Lima, D.R., Machado, F.M., dos Reis, G.S., da Silva, R.S., Pavan, F.A., Tran, H.N. Single-step pyrolysis for producing magnetic activated carbon from tucumã (*Astrocaryum aculeatum*) seed and nickel(II) chloride and zinc(II) chloride. Application for removal of Nicotinamide and Propanolol. J Hazard Mater 398 (2020) 122903. Doi:10.1016/j.jhazmat.2020.122903.

[44] Saucier, C., Karthickeyan, P., Ranjithkumar, V., Lima, E.C., dos Reis, G.S., de Brum, I.A.S. Efficient removal of amoxicillin and paracetamol from aqueous solutions using magnetic-activated carbon. Environ Sci Pollut Res 24 (2017) 5918-5932.

[45] Dos Reis, G.S., Sampaio, C.H., Lima, E.C., Wilhelm, M. Preparation of novel adsorbents based on combinations of polysiloxanes and sewage sludge to remove pharmaceuticals from aqueous solutions. Colloids Surf A: Physicochem Eng Aspects, 497 (2016) 304–315.

[46] Umpierres, C.S., Thue, P.S., dos Reis, G.S., de Brum, I.A.S., Lima, E.C., de Alencar, W.A., Dias, S.L.P., Dotto, G.L. Microwave activated carbons from Tucumã (*Astrocaryum aculeatum*) waste for efficient removal of 2-nitrophenol from aqueous solutions. Environ Technol 39 (2018) 1173-1187.

[47] Lima, D.R., Hosseini-Bandegharaei, A., Thue, P.S., Lima, E.C., de Albuquerque, Y.R.T., dos Reis, G.S., Umpierres, C.S., Dias, S.L.P., Tran, H.N. Efficient acetaminophen removal from water and hospital effluents treatment by activated carbons derived from Brazil nutshells. Colloids Surfaces A: Physicochem Eng Aspects 583 (2019) 123966. Doi:10.1016/j.colsurfa.2019.123966.

[48] Kasperiski, F.M., Lima, E.C., Umpierres, C.S., dos Reis, G.S., Thue, P.S., Lima, D.R. Dias, S.L.P., Saucier, C., da Costa, J.B. Production of porous activated carbons from *Caesalpinia ferrea* seed pod wastes: Highly efficient removal of Captopril from aqueous solutions. J Clean Prod 197 (2018) 919-929.

[49] Lima, E.C., Brasil, J.L., Santos, A.H.D.P. Evaluation of Rh, Ir, Ru, W-Rh, W-Ir, and W-Ru as Permanent Modifiers for the Determination of Lead in Ashes, Coals, Sediments, Sludges, Soils, and Freshwaters by Electrothermal Atomic Absorption Spectrometry. Anal Chim Acta, 484 (2003) 233-242.

[50] Lima, E.C., Barbosa Jr., F., Krug, F.J. The use of tungsten–rhodium permanent chemical modifier for cadmium determination in decomposed samples of biological materials and sediments by electrothermal atomic absorption spectrometry. Anal Chim Acta, 409 (2000) 267-274.

[51] Lima, E.C., Barbosa Jr., F., Krug, F.J., Guaita, U. Tungsten-Rhodium Permanent Chemical Modifier for Lead Determination in Digests of Biological Materials and Sediments by Electrothermal Atomic Absorption Spectrometry. J Anal At Spectrom 14 (1999) 1601-1605.

[52] Lima, E.C., Fenga, P.G., Romero, J.R., de Giovani, W.F. Electrochemical behavior of $[Ru(4,4'\text{-}Me_2bpy)_2(PPh_3)(H_2O)](ClO_4)_2$ in Homogeneous Solution and Incorporated into Carbon Paste Electrodes. Application to Oxidation of Benzylic Compounds. Polyhedron 17 (1998) 313-318.

[53] Lima, E.C., Adebayo, M.A., Machado, F.M. Chapter 3: Kinetic and Equilibrium Models of Adsorption, in Carbon Nanomaterials as Adsorbents for Environmental and Biological Applications, C.P. Bergmann, F.M. Machado, Eds. Springer International Publishing, 2015 pp. 33–69.

[54] Lima, E.C., Sher, F., Guleria, A., Saeb, M.R., Anastopoulos, I., Tran, H.N., Hosseini-Bandegharaei, A. Is one performing the treatment data of adsorption kinetics correctly? J Environ Chem Eng 9 (2021) 104813. doi:10.1016/j.jece.2020.104813.

[55] Lima, E.C., Hosseini-Bandegharaei, A., Moreno-Piraján, J.C., Anastopoulos, I., A critical review of the estimation of the thermodynamic parameters on adsorption equilibria.

Wrong use of equilibrium constant in the Van't Hoof equation for calculation of thermodynamic parameters of adsorption. J Mol Liq 273 (2019) 425-434.

[56] Lima, E.C. Hosseini-Bandegharaei, A, Anastopoulos, I. Response to "Some remarks on a critical review of the estimation of the thermodynamic parameters on adsorption equilibria. Wrong use of equilibrium constant in the van't Hoff equation for calculation of thermodynamic parameters of adsorption - Journal of Molecular Liquids 273 (2019) 425–434". J Mol Liq, 280 (2019) 298-300.

[57] Lima, E.C., Gomes, A.A., Tran, H.N. Comparison of the nonlinear and linear forms of the van't Hoff equation for calculation of adsorption thermodynamic parameters (ΔS° and ΔH°). J Mol Liq 311 (2020) 113315. Doi:10.1016/j.molliq.2020.113315.

[58] Zou, Y., Li, L., Tan, B, Ma, Y., Fang, L., Lu, C., Xu, Z. Silane modified epoxy coatings with low surface tension to achieve self-healing of wide damages. Progress in Organic Coatings 133 (2019) 357-367.

[59] Chang, R., Thoman-Jr, J.W. Chapter 17- Intermolecular forces, in Physical Chemistry for Chemical Sciences, University Science Books, 779-808, (2014).

[60] Lipkowski, P., Koll, A., Karpfen, A., Wolschann, P. An approach to estimate the energy of the intramolecular hydrogen bond. Chem. Phys. Lett. 10 (2002) 256-263.

Captions for Figures

Fig 1. Scheme of formation of hybrid.

Fig 2. FTIR spectra of AW@APTES-0.5 and AW.

Fig 3. TGA and DTA analysis. A- TGA of AW@APTES-0.5; B- DTA of AW@APTES-0.5; C- TGA of AW; D- DTA of AW.

Fig 4. Isotherm of adsorption (A, C) and pore size distribution curves (B, D).

Fig 5. pH_{pzc} A- AW@APTES-0.5, B- AW.

Fig 6. Kinetics of adsorption of 400 mg L^{-1} RB-4 onto AW@APTES-0.5 and AW adsorbents. A- nonlinear fitting using AW@APTES-0.5 adsorbent; B- intraparticle diffusion of RB-4 onto AW@APTES-0.5 adsorbent; C- nonlinear fitting using AW adsorbent; D- intraparticle diffusion of RB-4 onto AW adsorbent.

Fig 7. Mechanism of interaction between the adsorbent and adsorbate.

Fig 8. UV-Vis spectra before and after treatment with both adsorbents. A- Effluent A; B- Effluent-B. For the chemical composition of the effluents, see Table S1.

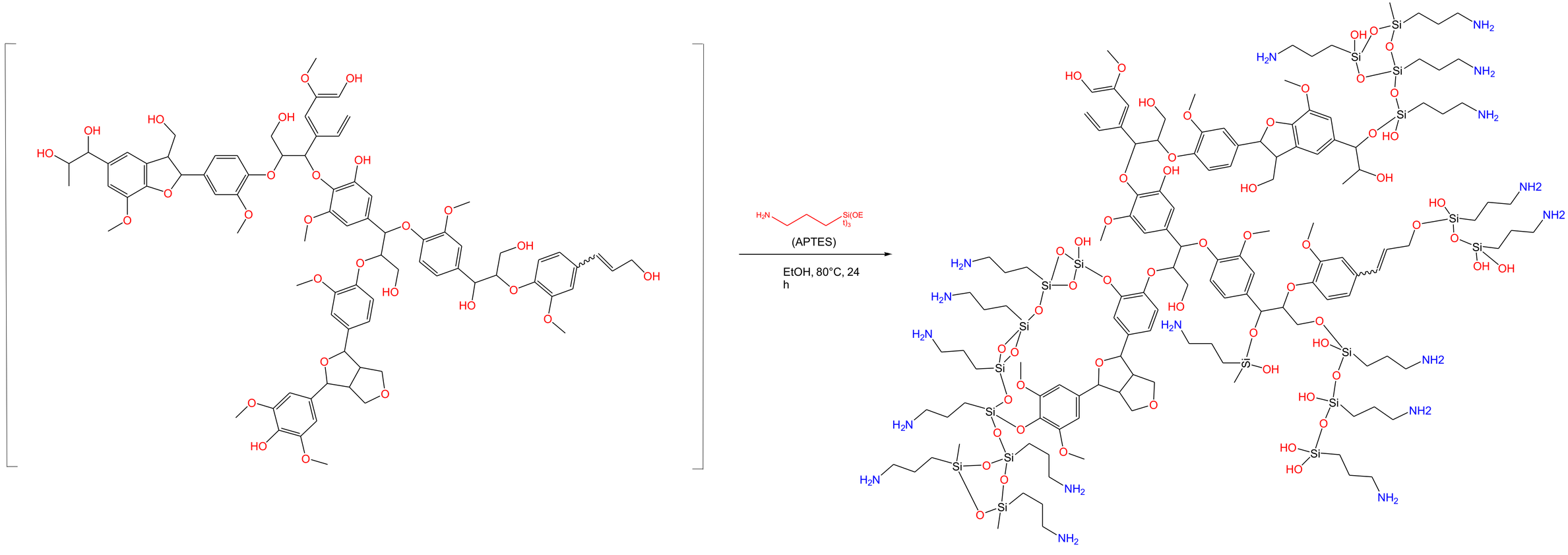

Fig 1

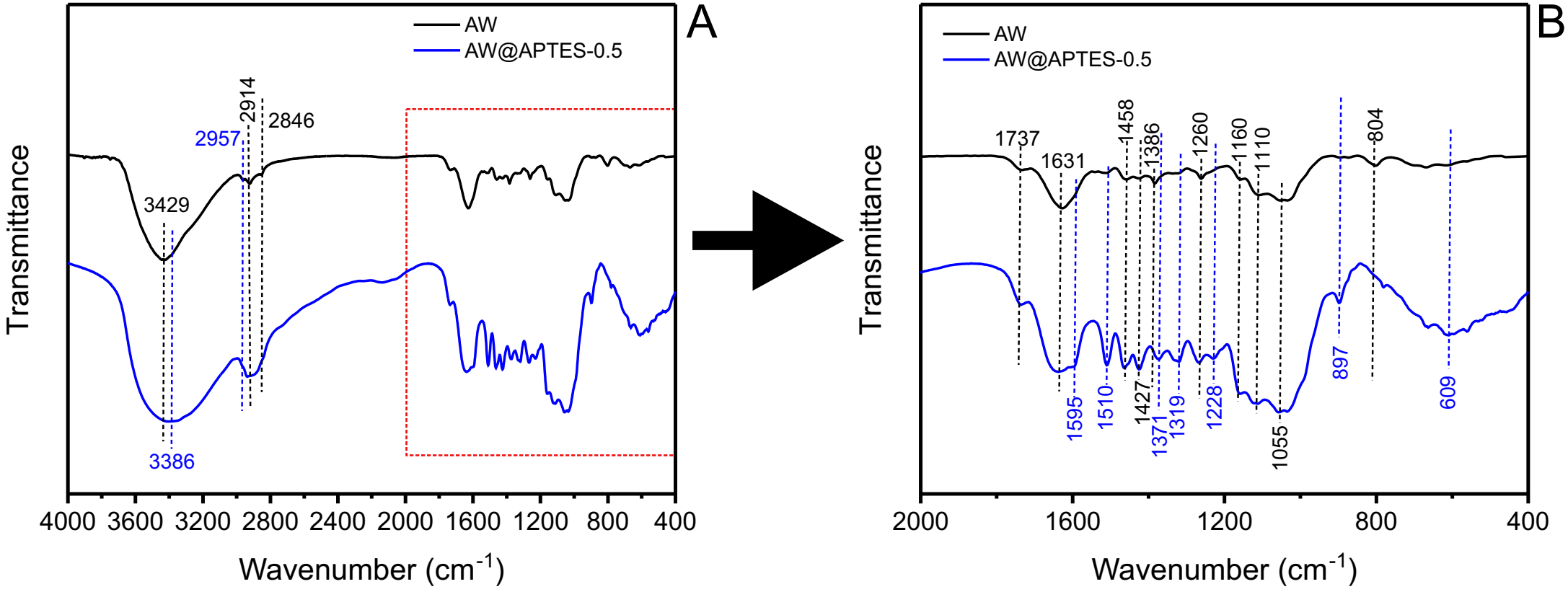
A
AW
AW@APTES-0.5
Transmittance
3429
2957
2914
2846
3386
4000 3600 3200 2800 2400 2000 1600 1200 800 400
Wavenumber (cm-1)
B
AW
AW@APTES-0.5
Transmittance
1737
1631
1595
1510
1458
1427
1386
1371
1319
1260
1228
1160
1110
1055
897
804
609
2000 1600 1200 800 400
Wavenumber (cm-1)

Fig 2

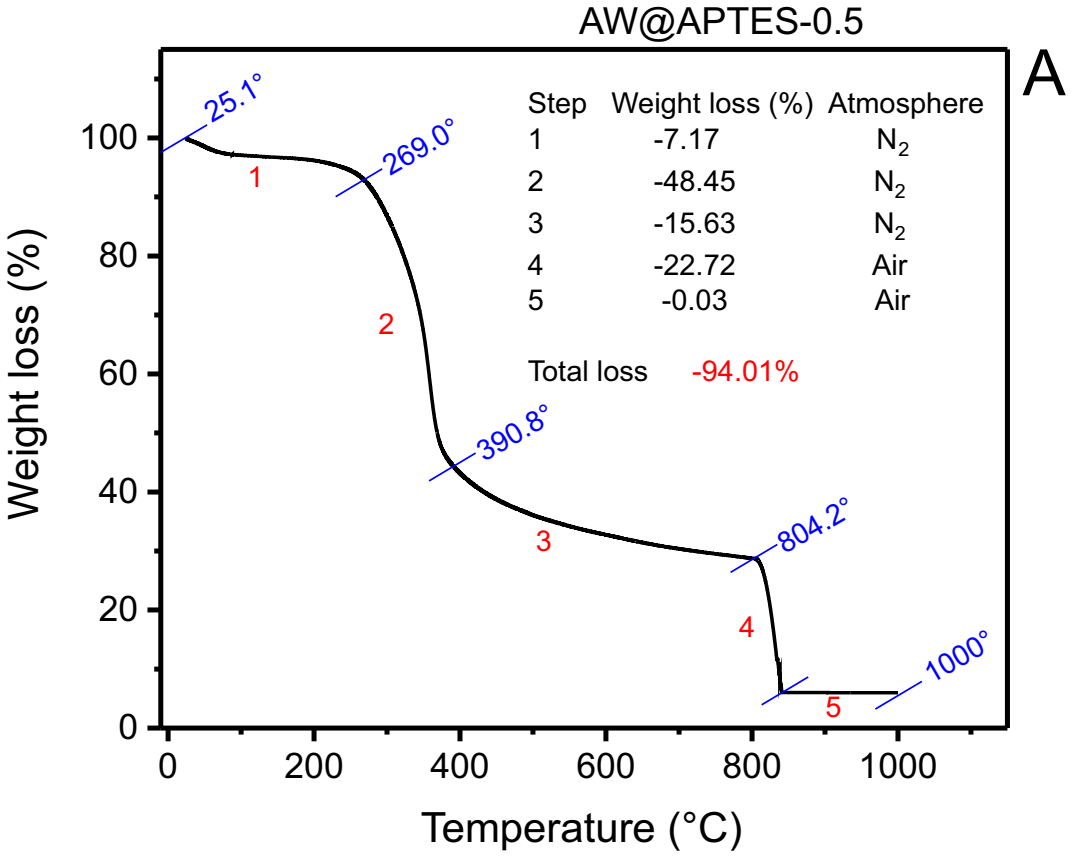
AW@APTES-0.5
A
Step Weight loss (%) Atmosphere
1 -7.17 N2
2 -48.45 N2
3 -15.63 N2
4 -22.72 Air
5 -0.03 Air
Total loss -94.01%
25.1°
269.0°
390.8°
804.2°
1000°
Weight loss (%)
Temperature (°C)

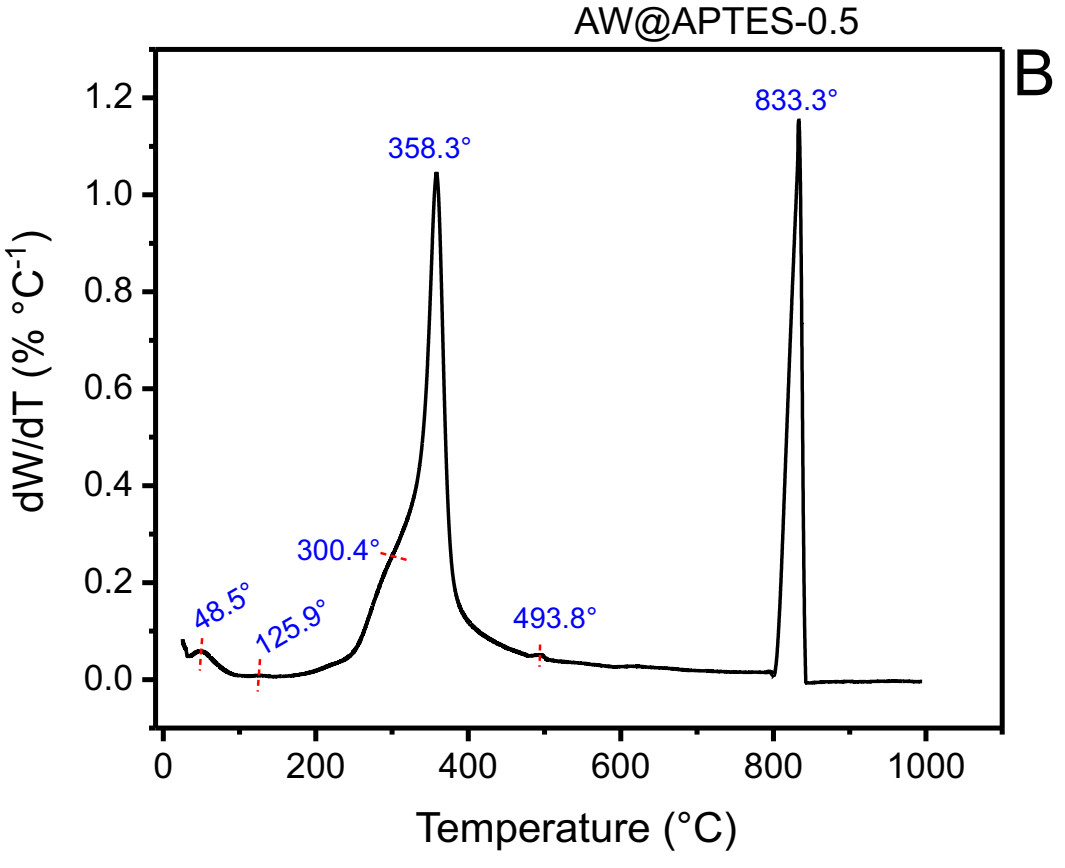
AW@APTES-0.5
B
358.3°
833.3°
300.4°
48.5°
125.9°
493.8°
dW/dT (% °C-1)
Temperature (°C)

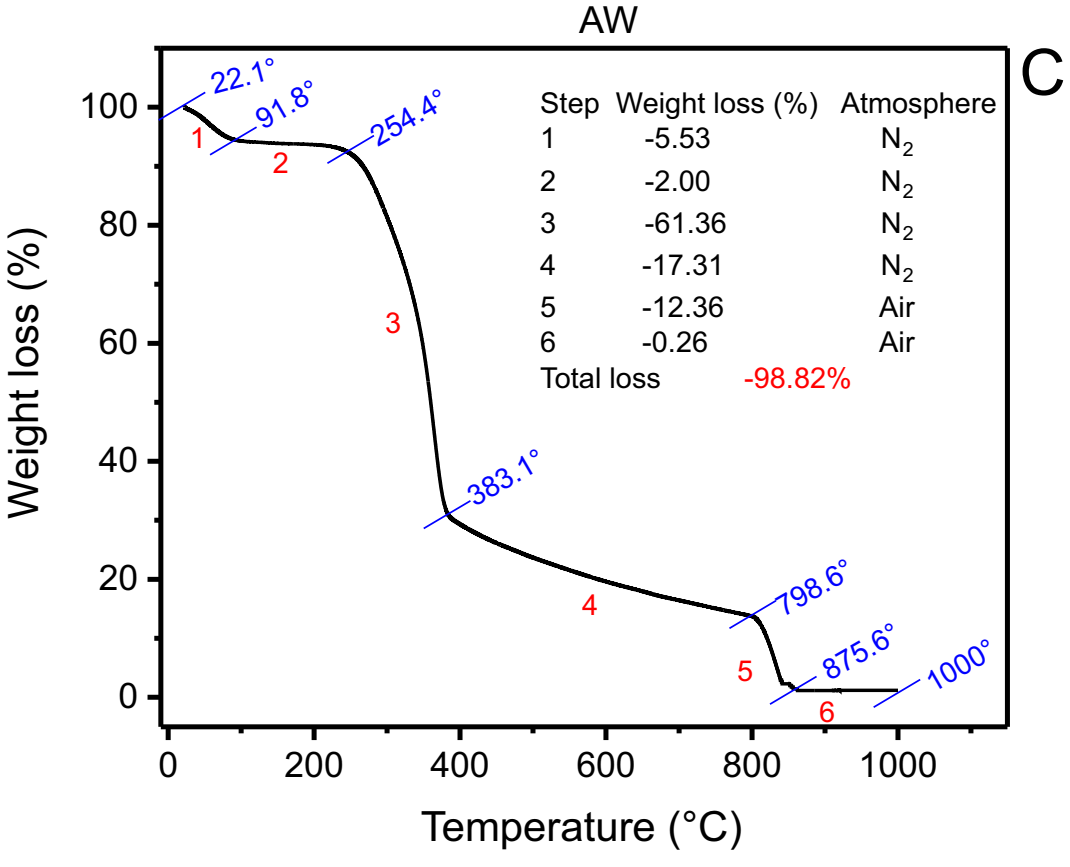
AW
C
Step Weight loss (%) Atmosphere
1 -5.53 N2
2 -2.00 N2
3 -61.36 N2
4 -17.31 N2
5 -12.36 Air
6 -0.26 Air
Total loss -98.82%
22.1°
91.8°
254.4°
383.1°
798.6°
875.6°
1000°
Weight loss (%)
Temperature (°C)

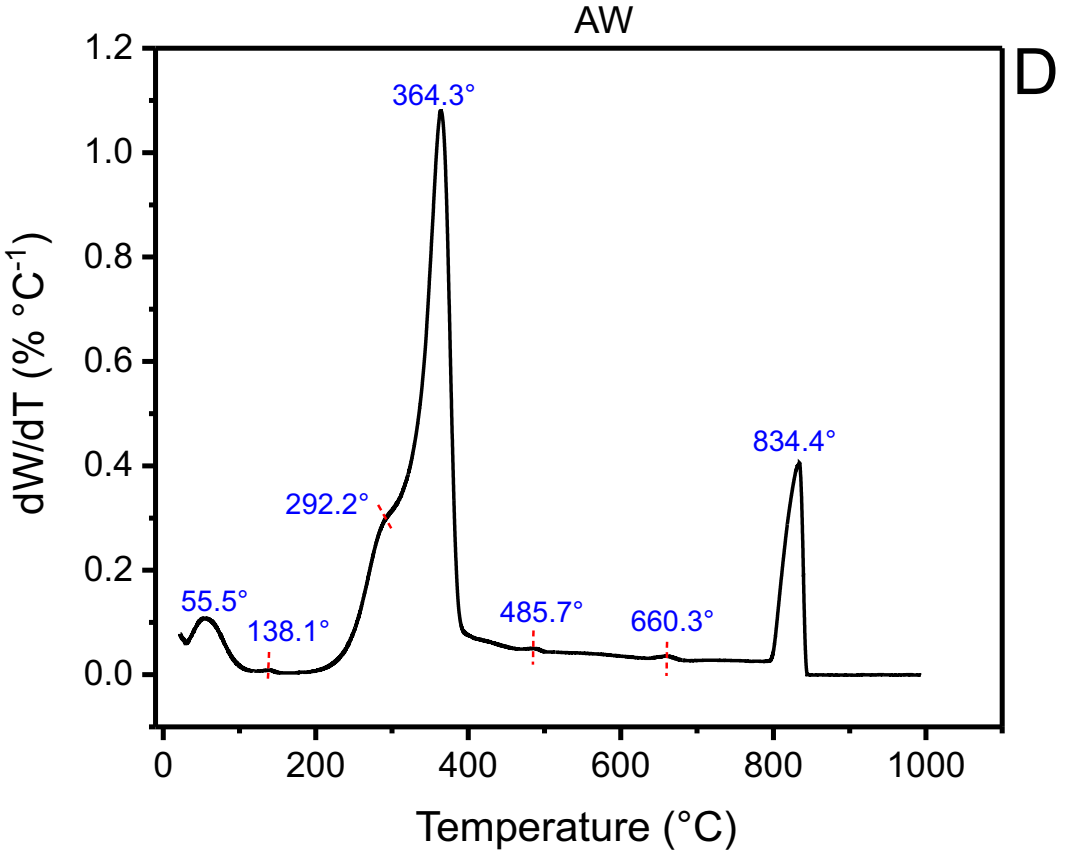
AW
D
364.3°
834.4°
292.2°
55.5°
138.1°
485.7°
660.3°
dW/dT (% °C-1)
Temperature (°C)

Fig 3

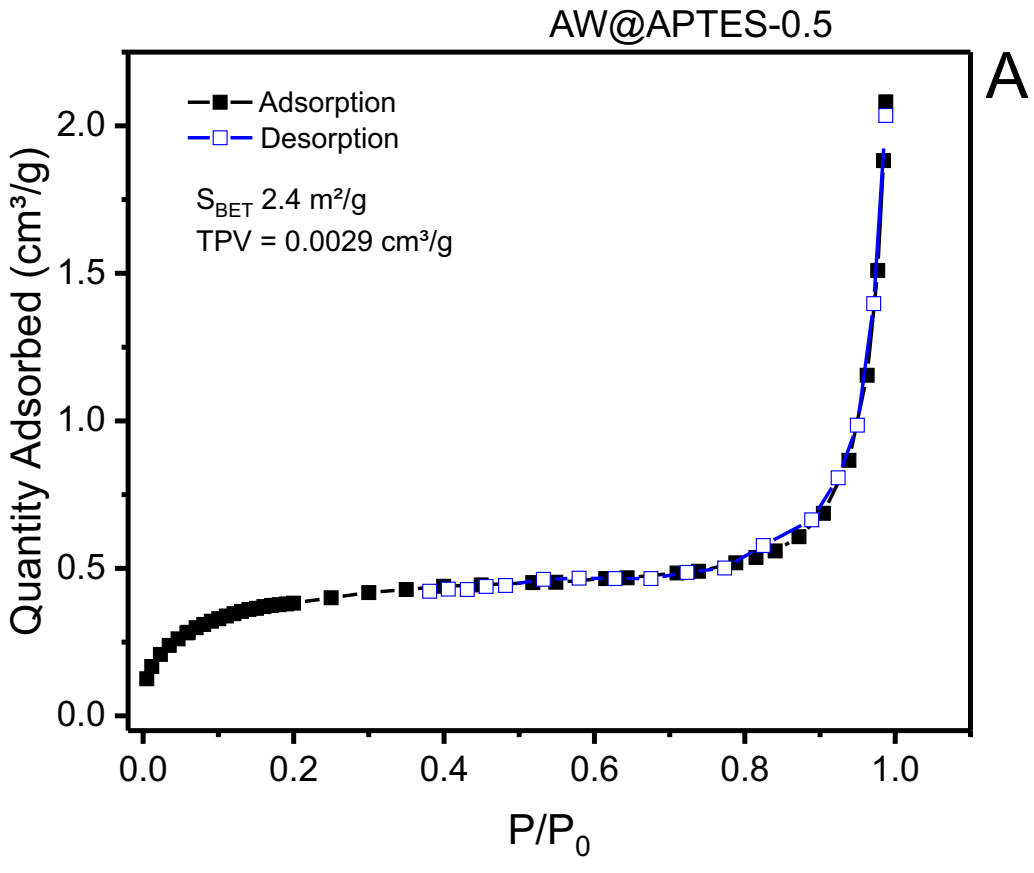
AW@APTES-0.5
A
Adsorption
Desorption
S_{BET} 2.4 m²/g
TPV = 0.0029 cm³/g
Quantity Adsorbed (cm³/g)
P/P0
0.0
0.5
1.0
1.5
2.0
0.2
0.4
0.6
0.8

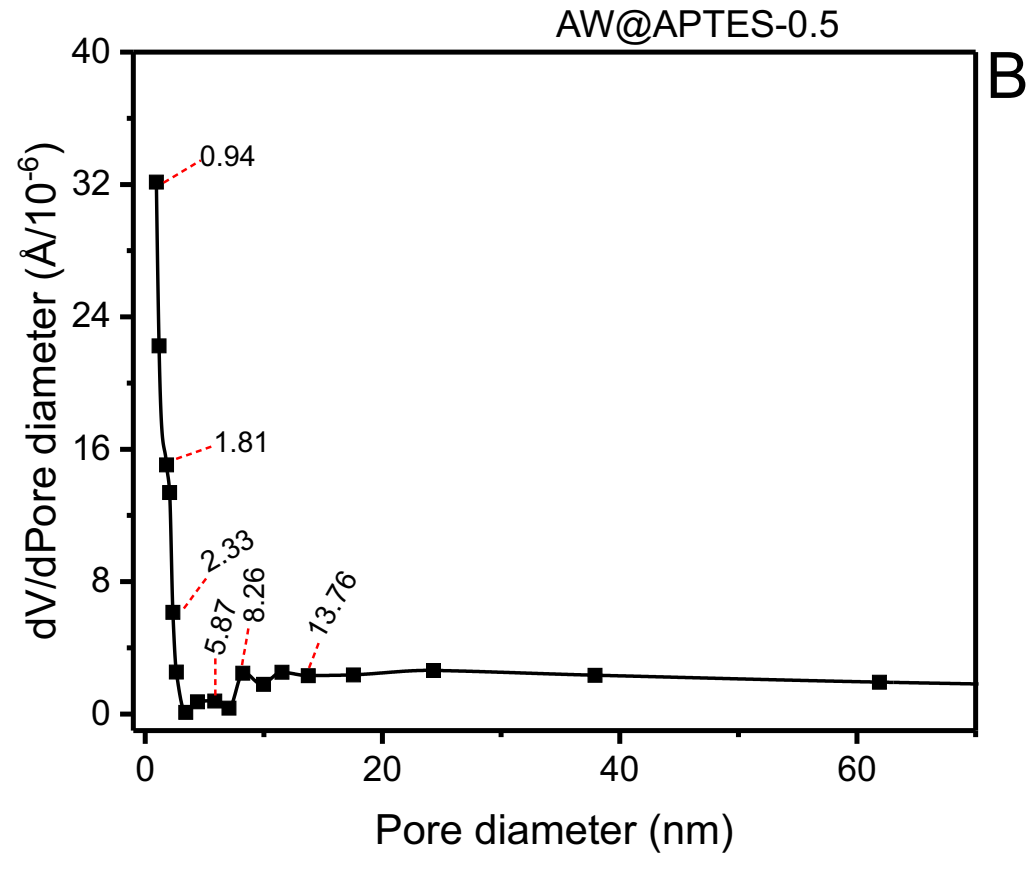
AW@APTES-0.5
B
dV/dPore diameter (Å/10-6)
Pore diameter (nm)
0.94
1.81
2.33
5.87
8.26
13.76
0
8
16
24
32
40
20
60

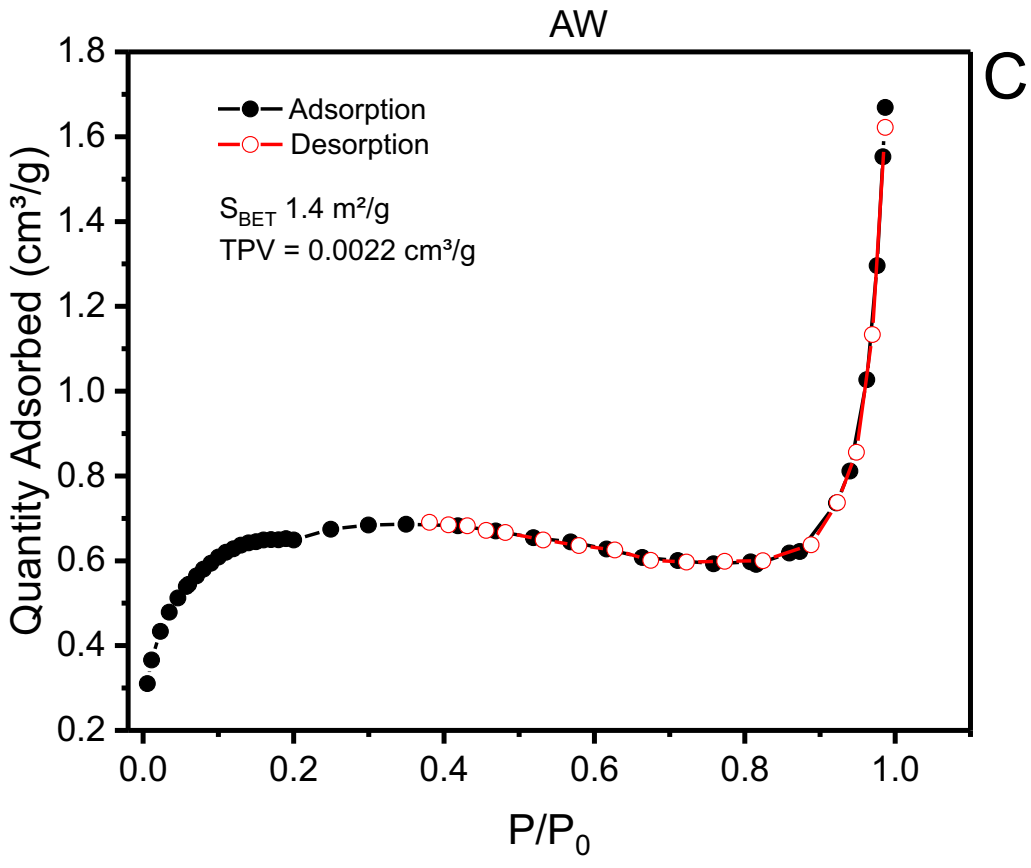
AW
C
Adsorption
Desorption
S_{BET} 1.4 m²/g
TPV = 0.0022 cm³/g
Quantity Adsorbed (cm³/g)
P/P0
0.2
0.4
0.6
0.8
1.0
1.2
1.4
1.6
1.8
0.0
0.2
0.4
0.6
0.8
1.0

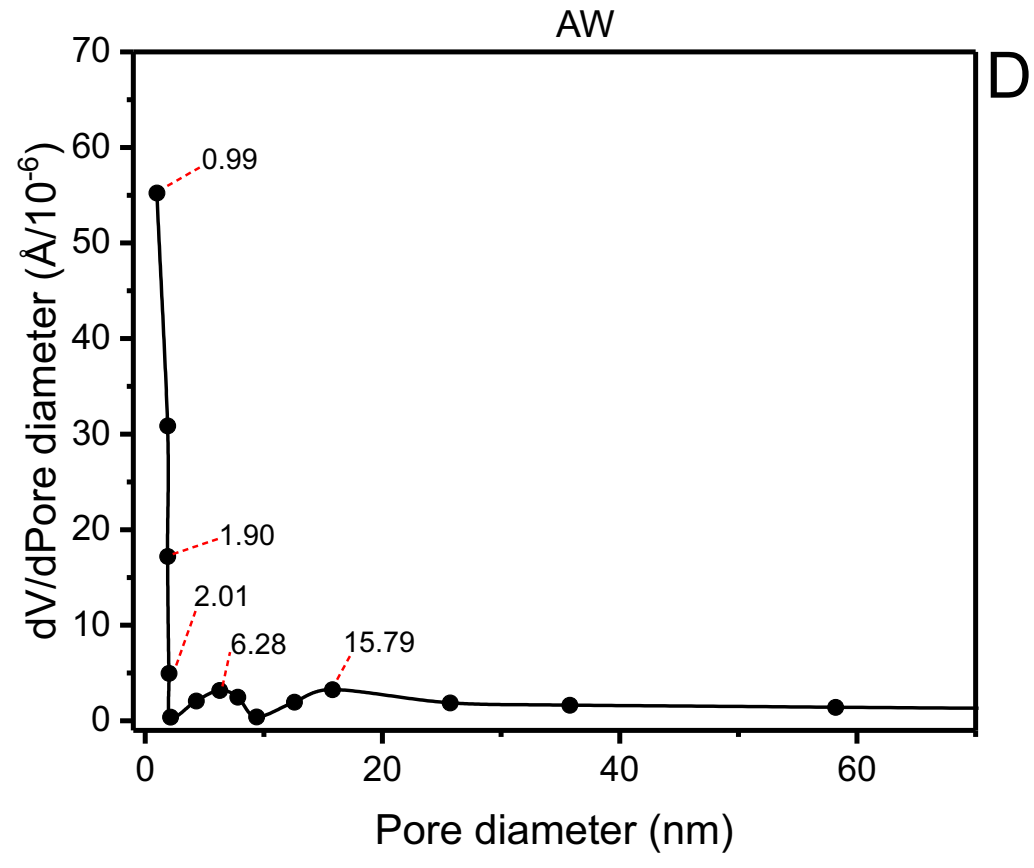
AW
D
dV/dPore diameter (Å/10-6)
Pore diameter (nm)
0.99
1.90
2.01
6.28
15.79
0
10
20
30
40
50
60
70
20
40
60

Fig 4

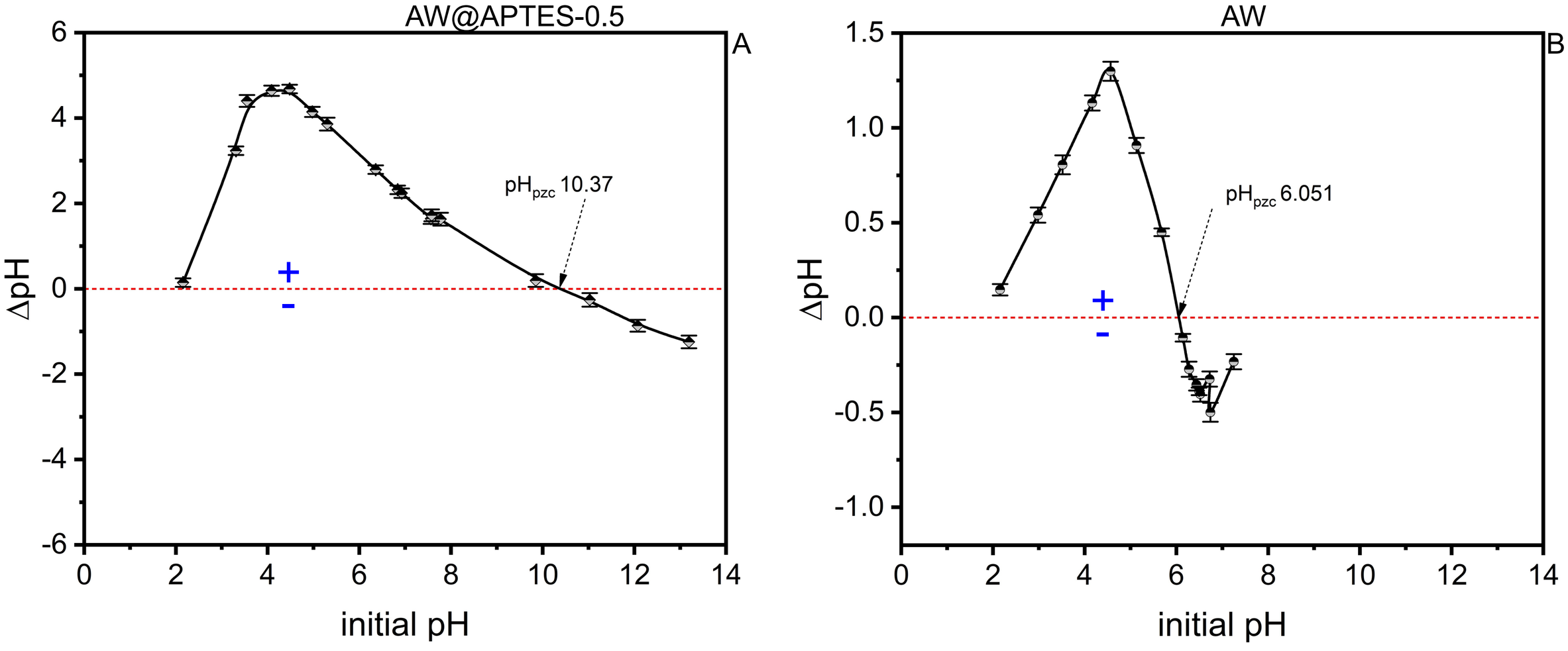
AW@APTES-0.5
A
pHpzc 10.37
+
-
ΔpH
initial pH
AW
B
pHpzc 6.051
+
-
ΔpH
initial pH

Fig 5

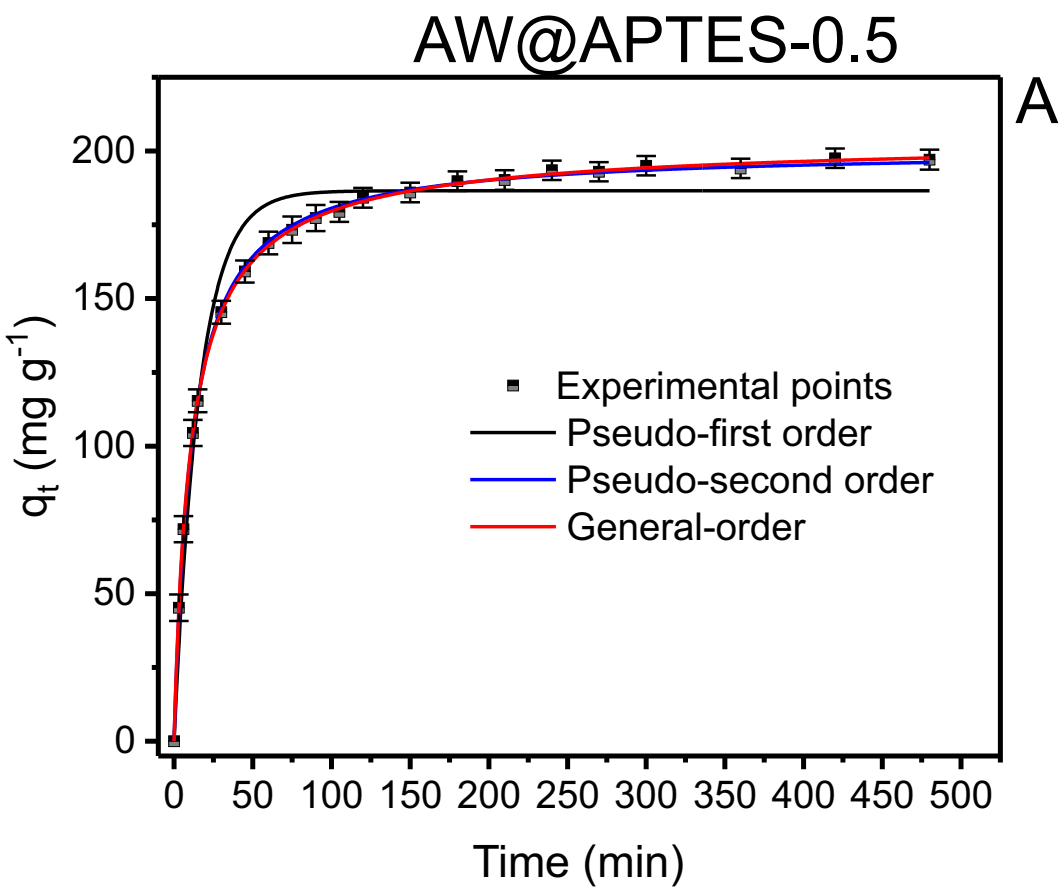
AW@APTES-0.5
A
q_t (mg g^{-1})
Time (min)
Experimental points
Pseudo-first order
Pseudo-second order
General-order

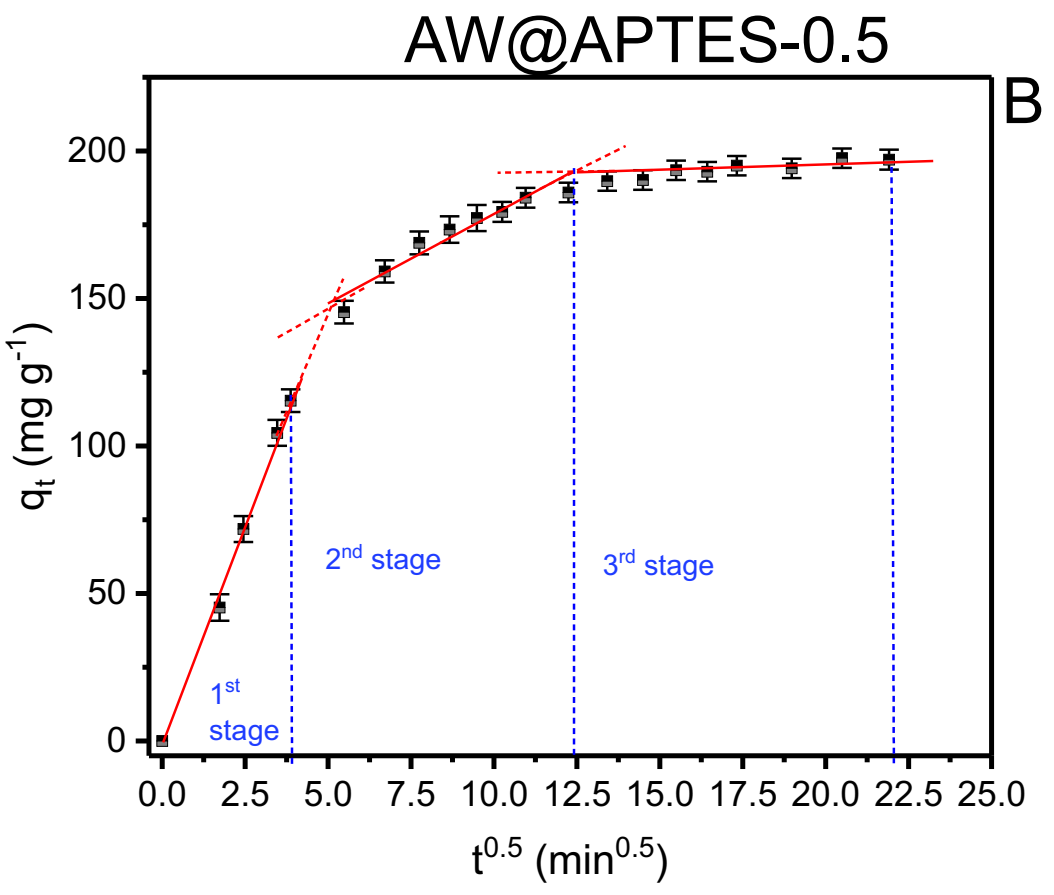
AW@APTES-0.5
B
q_t (mg g^{-1})
$t^{0.5}$ ($min^{0.5}$)
1st stage
2nd stage
3rd stage

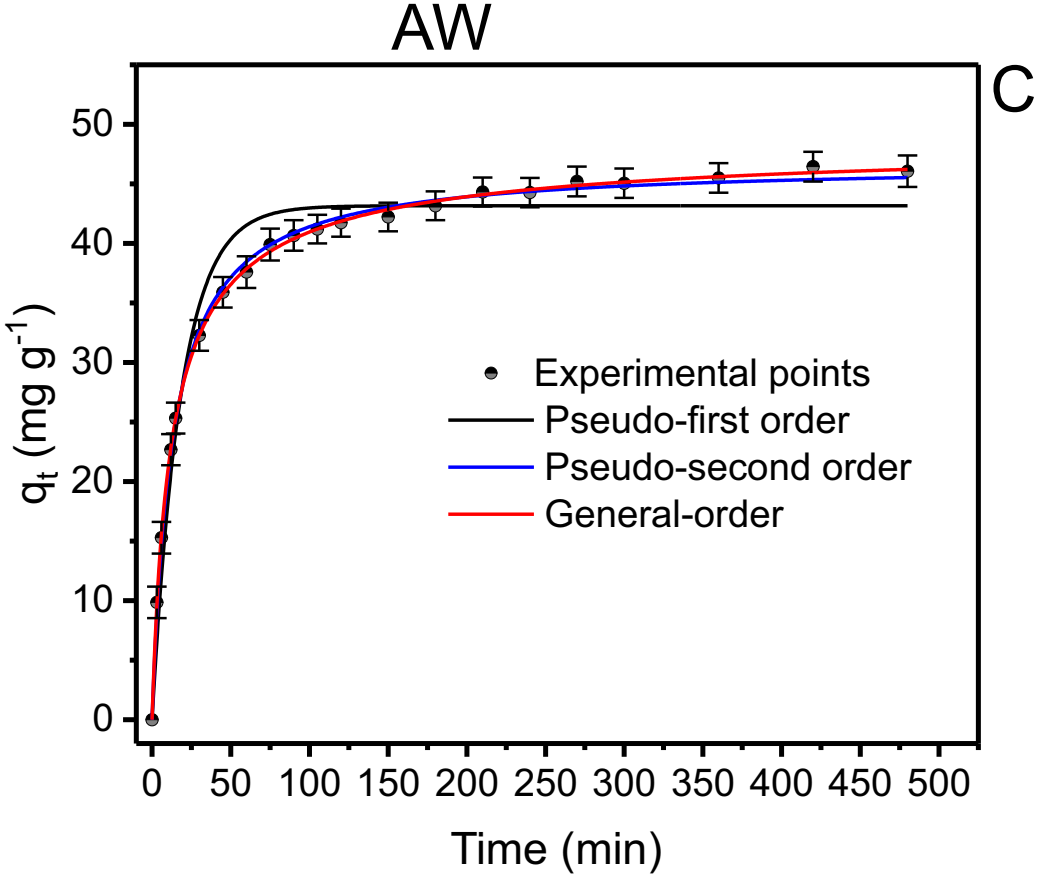
AW
C
q_t (mg g^{-1})
Time (min)
Experimental points
Pseudo-first order
Pseudo-second order
General-order

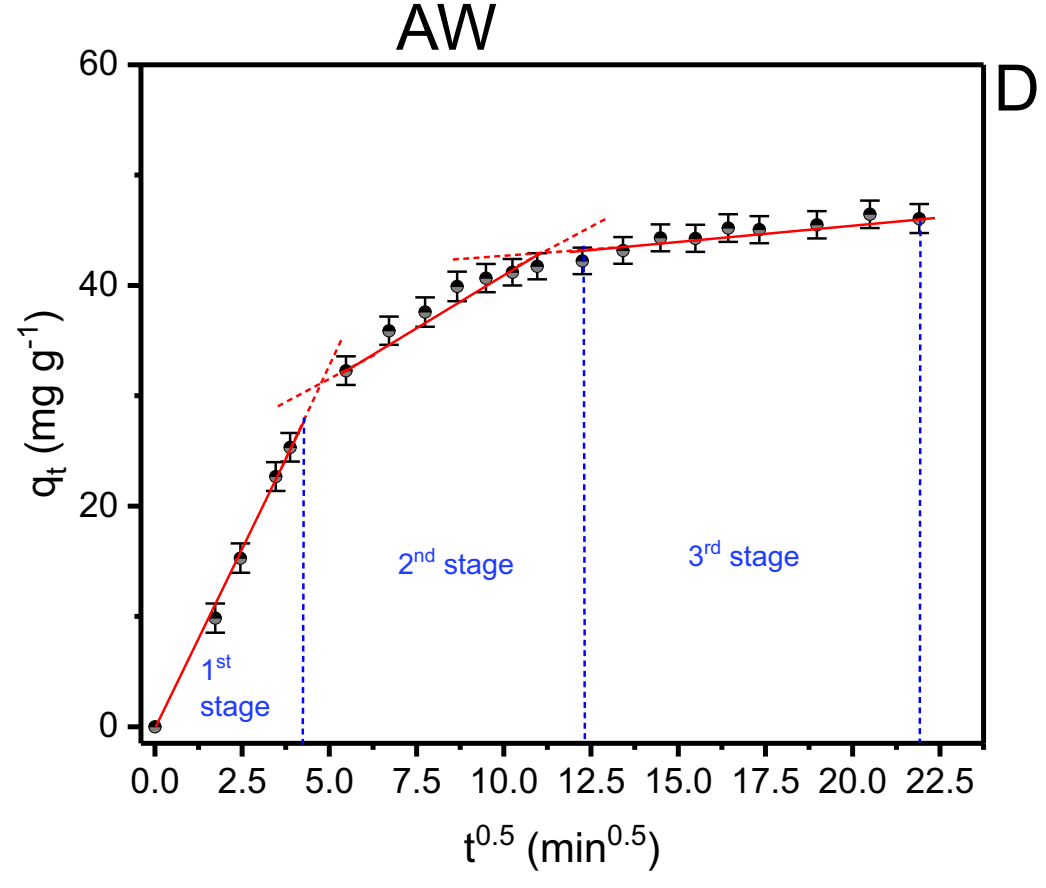
AW
D
q_t (mg g^{-1})
$t^{0.5}$ ($min^{0.5}$)
1st stage
2nd stage
3rd stage

Fig 6

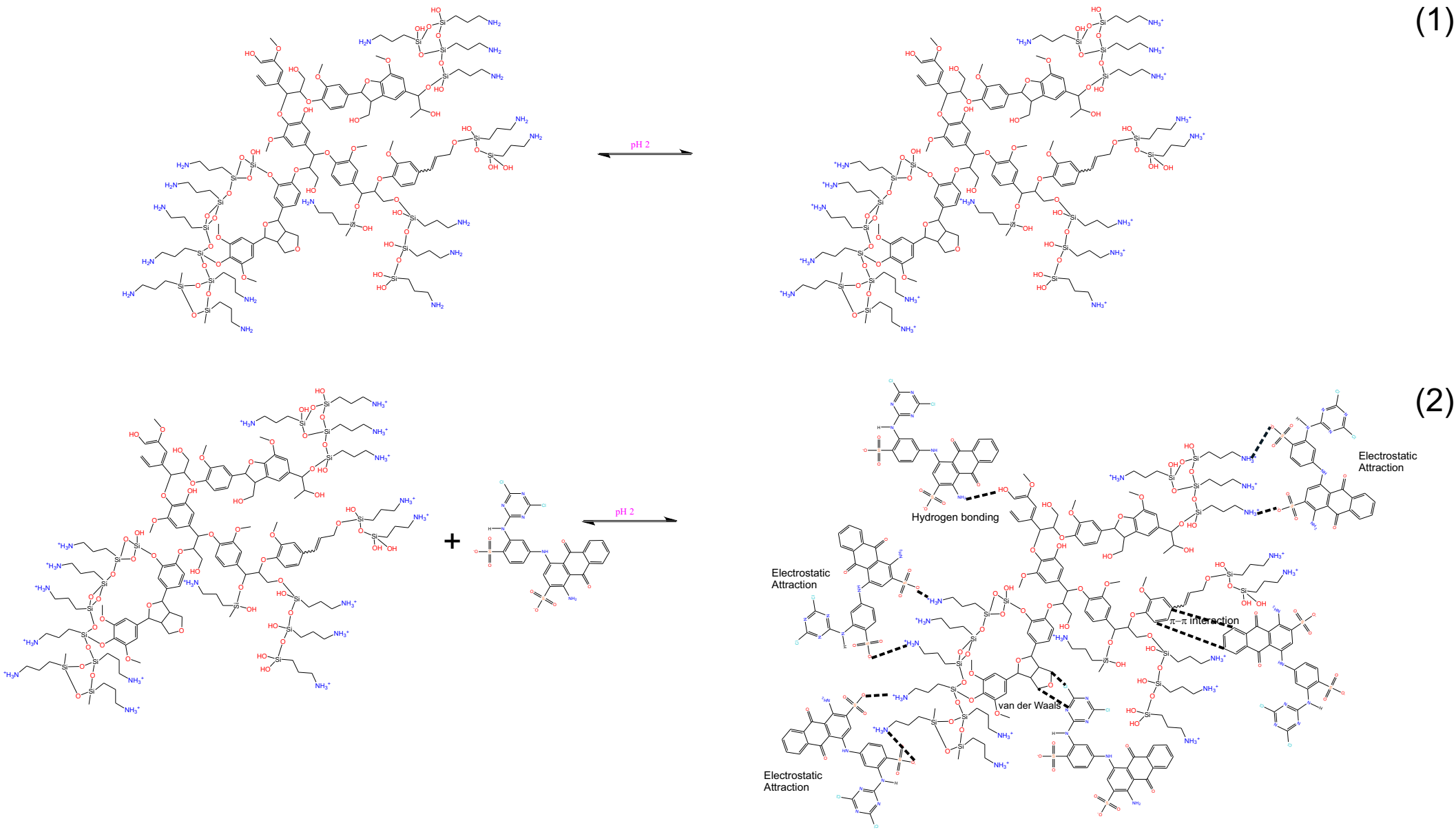
(1)
pH 2
(2)
pH 2
Hydrogen bonding
Electrostatic Attraction
Electrostatic Attraction
π−π interaction
van der Waals
Electrostatic Attraction

Fig 7

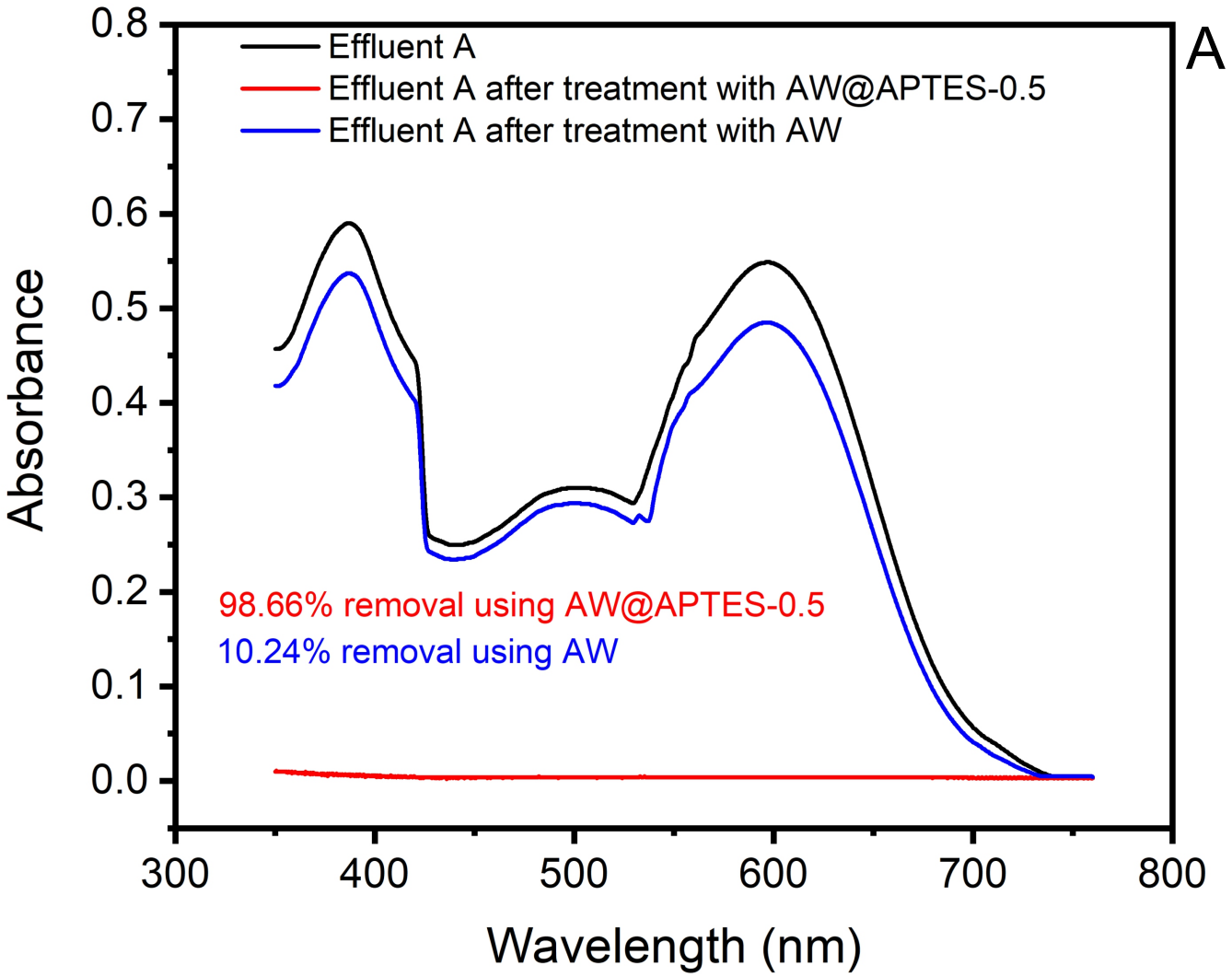
A
Effluent A
Effluent A after treatment with AW@APTES-0.5
Effluent A after treatment with AW
98.66% removal using AW@APTES-0.5
10.24% removal using AW
Absorbance
Wavelength (nm)
0.0
0.1
0.2
0.3
0.4
0.5
0.6
0.7
0.8
300
400
500
600
700
800

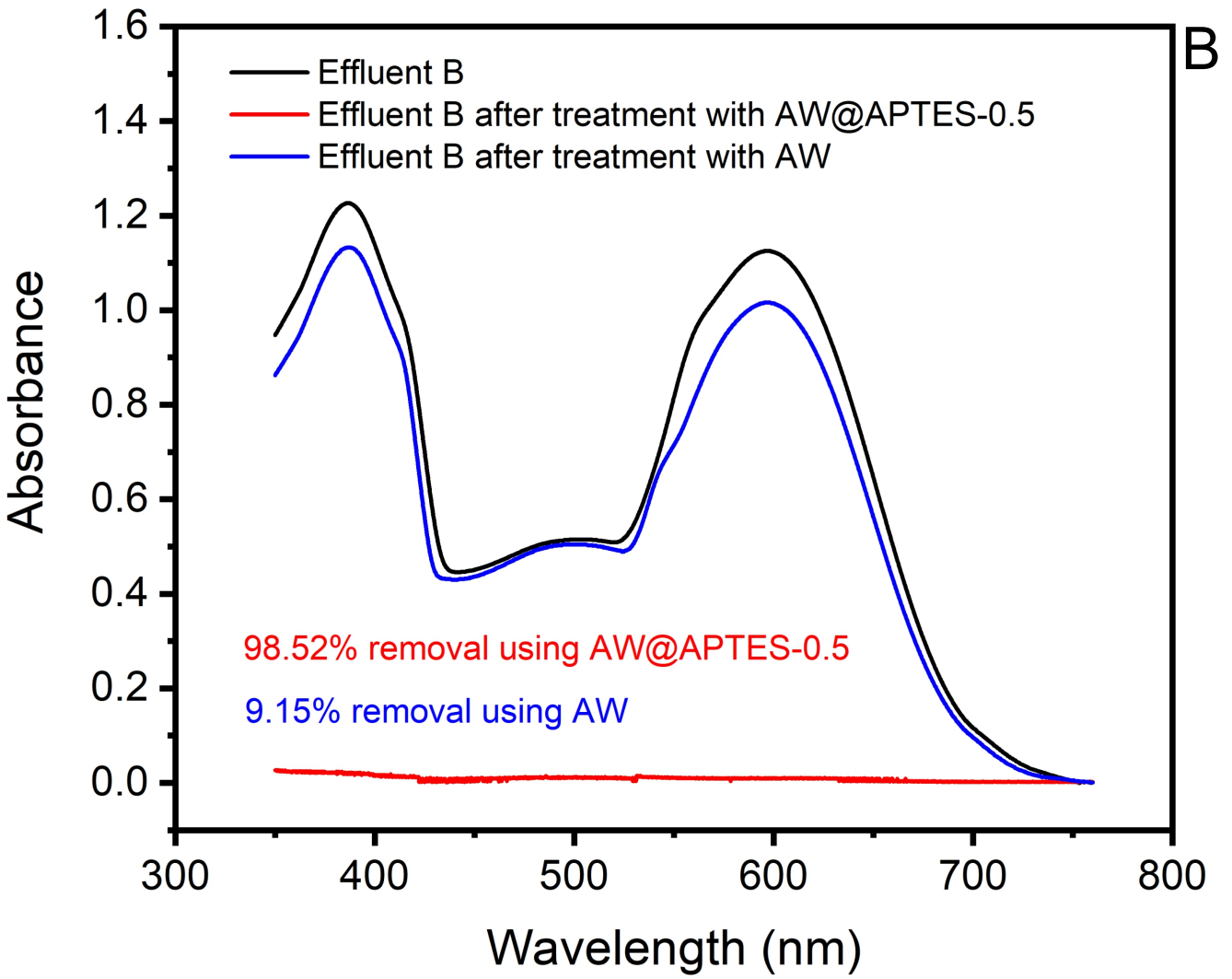
B
Effluent B
Effluent B after treatment with AW@APTES-0.5
Effluent B after treatment with AW
98.52% removal using AW@APTES-0.5
9.15% removal using AW
Absorbance
Wavelength (nm)
0.0
0.2
0.4
0.6
0.8
1.0
1.2
1.4
1.6
300
400
500
600
700
800

Fig 8

Supplementary Material

Preparation of hybrids of wood sawdust with 3-aminopropyl-triethoxysilane. Application as an adsorbent to remove Reactive Blue 4 dye from wastewater effluents.

Roberta A. Teixeira, Eder C. Lima, Antônio D. Benetti, Pascal S. Thue, Mariene R. Cunha, Nilton F.G.M. Cimirro, Diana R. Lima, Faroq Sher, Mohammad Hadi Dehghani

2.5. Models of kinetics and isotherms of adsorption

Pseudo-first-order [53], pseudo-second-order [53], and General-order [53] models were used to fit the kinetic data. The mathematical equations of these respective models are shown in Equations 8, 9, and 10.

$$q_t = q_e \cdot \left[1\text{-}exp(\text{-}k_1 \cdot t)\right] \quad (8)$$

$$q_t = \frac{q_e^2 k_2 t}{\left[k_2 (q_e) \cdot t + 1\right]} \quad (9)$$

$$q_t = q_e - \frac{q_e}{\left[k_N (q_e)^{n-1} \cdot t \cdot (n\text{-}1) + 1\right]^{1/1-n}} \quad (10)$$

Where t is the contact time (min); q_t, q_e are the amount of adsorbate adsorbed at time t and the equilibrium respectively (mg g^{-1}); k_1 is the pseudo-first-order rate constant (min^{-1}); k_2 is the pseudo-second-order rate constant (g mg^{-1} min^{-1}); k_N is the general order constant rate (min^{-1}.(g mg^{-1})$^{n-1}$), n is the general-order exponent ($n \neq 1$) .

Langmuir, Freundlich, and Liu's models were employed for the analysis of equilibrium data. Equations 11, 12 and 13 show the corresponding Langmuir [53], Freundlich [53], and Liu models [53].

$$q_e = \frac{Q_{\max} \cdot K_L \cdot C_e}{1 + K_L \cdot C_e} \quad (11)$$

$$q_e = K_F \cdot C_e^{1/n_F} \quad (12)$$

$$q_e = \frac{Q_{\max} \cdot (K_g \cdot C_e)^{n_L}}{1 + (K_g \cdot C_e)^{n_L}} \quad (13)$$

Where q_e is the adsorbate amount adsorbed at equilibrium (mg g^{-1}); C_e is the adsorbate concentration at equilibrium (mg L^{-1}); Q_{max} is the maximum sorption capacity of the adsorbent (mg g^{-1}); K_L is the Langmuir equilibrium constant (L mg^{-1}); K_F is the Freundlich equilibrium constant [$mg.g^{-1}.(mg.L^{-1})^{-1/nF}$]; K_g is the Liu equilibrium constant (L mg^{-1}); n_F and n_L are the exponents of Freundlich and Liu model, respectively, (n_F and n_L are dimensionless).

Table S1. Chemical composition of the simulated dye effluents.

Dyes		**Concentration (mg L^{-1})**	
	λ_{max} (nm)	**Effluent A**	**Effluent B**
Procion Blue MX-R	594.0	45.00	90.00
Cibacron Brilliant Yellow 3G-P	402.0	12.00	24.00
Reactive Black 5	597.5	12.00	24.00
Reactive Orange 16	493.0	12.00	24.00
Reactive Red194	505.0	12.00	24.00
Other compounds			
Na_2CO_3		15.00	30.00
NaCl		15.00	30.00
CH_3COONa		15.00	30.00
KNO_3		15.00	30.00
Na_3PO_4		15.00	30.00
Sodium Dodecyl Sulfate		10.00	20.00
Na_2SO_4		10.00	20.00
NH_4Cl		10.00	20.00
Humic acid		10.00	20.00
pH*		2.0	2.0

*****pH of the solution was adjusted with 0.1 mol L^{-1} NaOH and or HCl.

Table S2. Hydrophobic/hydrophilic balance (HI) for AW and AW@APTES-X adsorbents.

Sample	HI*
AW	0.724
AW@APTES-0.25	0.326
AW@APTES-0.50	0.277
AW@APTES-1.0	0.324
AW@APTES-1.5	0.931
AW@APTES-2.0	0.868

Table S3. CHN elemental analysis for AW and AW@APTES-0.5.

	C (%)	H (%)	N (%)
AW	46.25	6.16	0.00
AW@APTES-0.5	44.53	6.12	1.00

Table S4. Kinetic parameters for adsorption of RB-4 dye onto AW and AW@APTES-0.5 adsorbents. It was used initial concentrations of 415 mg L^{-1} RB-4, the adsorbent dosage of 1.5 g L^{-1}, pH 2.

Pseudo-first order	AW@APTES-0.5	AW
q_e (mg g^{-1})	186.5	43.16
k_1 (min^{-1})	0.06265	0.05455
$t_{1/2}$ (min)	11.06	12.71
$t_{0.95}$ (min)	47.82	54.92
R^2_{adj}	0.9710	0.9659
SD (mg g^{-1})	9.543	2.442
BIC	101.8	62.05
Pseudo-second order		
q_e(mg g^{-1})	200.7	46.76
k_2(g mg^{-1} min^{-1})	$4.489.10^{-4}$	$1.652.10^{-3}$
$t_{1/2}$ (min)	10.61	12.28
$t_{0.95}$ (min)	144.2	159.8
R^2_{adj}	0.9994	0.9982
SD (mg g^{-1})	1.341	0.5574
BIC	19.37	-17.52
General-order		
q_e (mg g^{-1})	204.9	49.00
k_N (min^{-1}.(g mg^{-1})$^{n-1}$)	$1.562.10^{-4}$	$3.388.10^{-4}$
n	2.204	2.418
$t_{1/2}$ (min)	10.59	12.29
$t_{0.95}$ (min)	164.9	198.8
R^2_{adj}	0.9998	0.9994
SD (mg g^{-1})	0.8205	0.3157
BIC	0.6310	-39.48

Table S5. Parameters of the isotherm of Langmuir, Freundlich, and Liu for the uptake of RB-4 onto AW@APTES-0.5 and AW adsorbent.

AW@APTES-0.5	10°C	20°C	25°C	30°C	40°C	50°C
Langmuir						
Q_{max} (mg g^{-1})	294.4	348.1	349.0	395.2	384.8	423.2
K_L (L mg^{-1})	0.008461	0.01069	0.01327	0.01661	0.02299	0.03291
R^2_{adj}	0.9976	0.9789	0.9927	0.8970	0.9989	0.9983
SD (mg g^{-1})	4.034	14.40	8.702	36.878	3.793	5.317
BIC	47.82	85.99	70.89	114.2	45.97	56.10
Freundlich						
K_F [(mg g^{-1}) (mg L^{-1})^{nF}]	30.64	42.93	50.32	76.47	72.11	100.9
n_F	3.088	3.272	3.478	4.073	3.811	4.350
R^2_{adj}	0.9392	0.8866	0.9064	0.7667	0.9253	0.9133
SD (mg g^{-1})	20.30	33.38	31.13	55.51	31.15	37.68
BIC	96.30	111.2	109.1	126.5	109.1	114.9
Liu						
Q_{max} (mg g^{-1})	276.8	306.3	321.9	338.3	373.2	415.1
K_g (L mg^{-1})	0.009478	0.01289	0.01504	0.01767	0.02441	0.03363
n_L	1.189	1.620	1.337	3.0712	1.115	1.089
R^2_{adj}	0.9999	0.9999	0.9999	0.9998	0.9999	0.9988
SD (mg g^{-1})	0.6006	1.191	0.4816	1.780	0.6760	4.516
BIC	-7.810	12.73	-14.43	24.78	-4.263	52.71
AW	10°C	20°C	25°C	30°C	40°C	50°C
Langmuir						
Q_{max} (mg g^{-1})	22.32	39.86	44.08	31.71	40.26	32.44
K_L (L mg^{-1})	0.00141	0.002877	0.003324	0.008018	0.005836	0.01297
R^2_{adj}	0.8805	0.9904	0.9876	0.9944	0.9947	0.9924
SD (mg g^{-1})	1.601	0.9847	1.253	0.6843	0.8345	0.8677
BIC	20.10	5.515	12.74	-5.402	0.5482	1.719
Freundlich						
K_F (mg g^{-1} (mg L^{-1})$^{-1/nF}$)	0.2520	1.300	1.922	3.527	3.102	5.217
n_F	1.750	2.200	2.399	3.269	2.833	3.842
R^2_{adj}	0.8311	0.9427	0.9348	0.9784	0.9370	0.9677
SD (mg g^{-1})	1.904	2.405	0.9348	1.350	2.884	1.788
BIC	25.29	32.30	37.67	14.98	37.76	23.42
Liu						
Q_{max} (mg g^{-1})	12.81	32.93	36.45	36.63	36.45	36.66
K_g (L mg^{-1})	0.003198	0.004168	0.004790	0.005460	0.007178	0.009486
n_L	4.186	1.439	1.523	0.7460	1.303	0.7227
R^2_{adj}	0.9999	0.9999	0.9999	0.9999	0.9999	0.9999
SD (mg g^{-1})	0.05419	0.07723	0.08141	0.02013	0.1363	0.05826
BIC	-79.97	-69.35	-67.76	-109.7	-52.30	-77.80

Table S6. Thermodynamics of adsorption of RB-4 dye onto AW@APTES-0.5 and AW. According to the literature, the thermodynamic equilibrium constant was calculated by the Liu isotherm of Table 4 [55,56]. The ΔH° and ΔS° were calculated using nonlinear fitting [57].

AW@APTES-0.5						
T (K)	283	293	298	303	313	323
K_e	$6.042.10^3$	$8.219.10^3$	$9.586.10^3$	$1.126.10^4$	$1.556.10^4$	$2.144.10^4$
ΔG^Θ (kJ mol^{-1})	-20.49	-21.96	-22.71	-23.50	-25.12	-26.78
ΔS^Θ (J $K^{-1}.mol^{-1}$)	-	-	160.6	-	-	-
ΔH^Θ (kJ mol^{-1})	-	-	25.10	-	-	-

AW						
T (K)	283	293	298	303	313	323
K_e	$2.038.10^3$	$2.657.10^3$	$3.053.10^3$	$3.481.10^3$	$4.575.10^3$	$6.047.10^3$
ΔG^Θ (kJ mol^{-1})	-17.93	-19.21	-19.88	-20.54	-21.93	-23.38
ΔS^Θ (J $K^{-1}.mol^{-1}$)	-	-	138.5	-	-	-
ΔH^Θ (kJ mol^{-1})	-	-	21.37	-	-	-

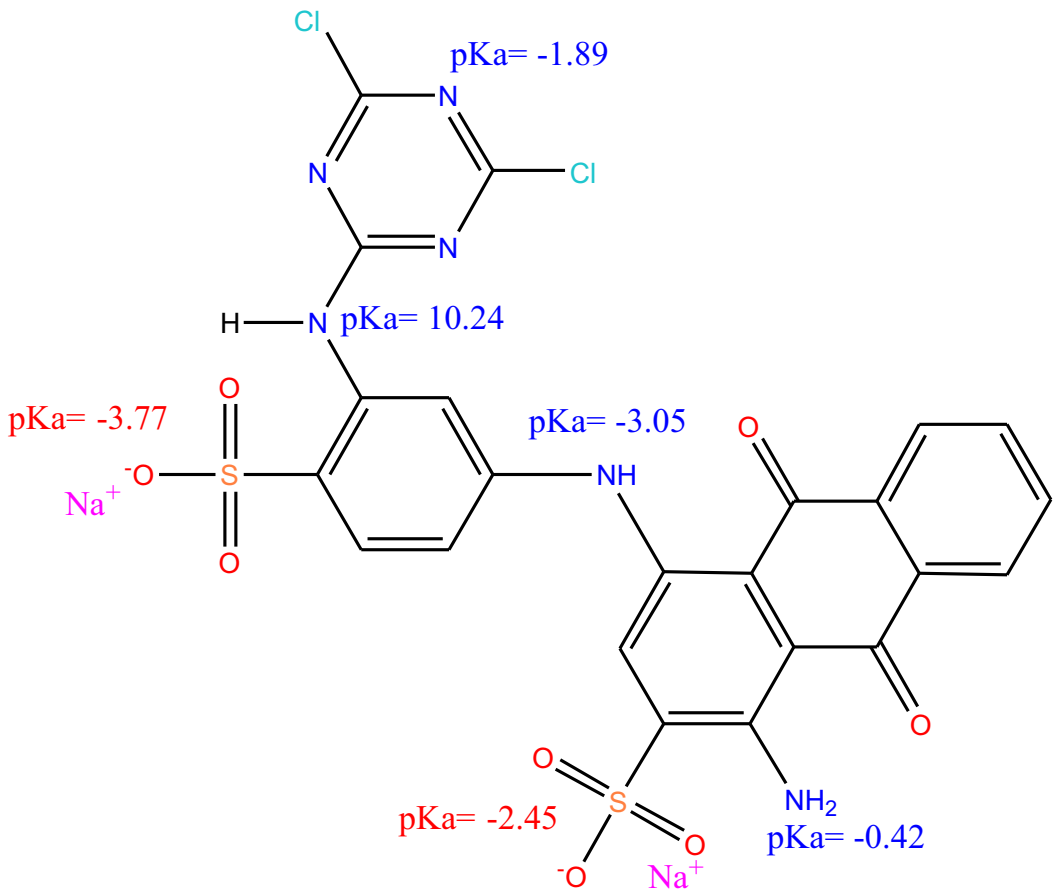

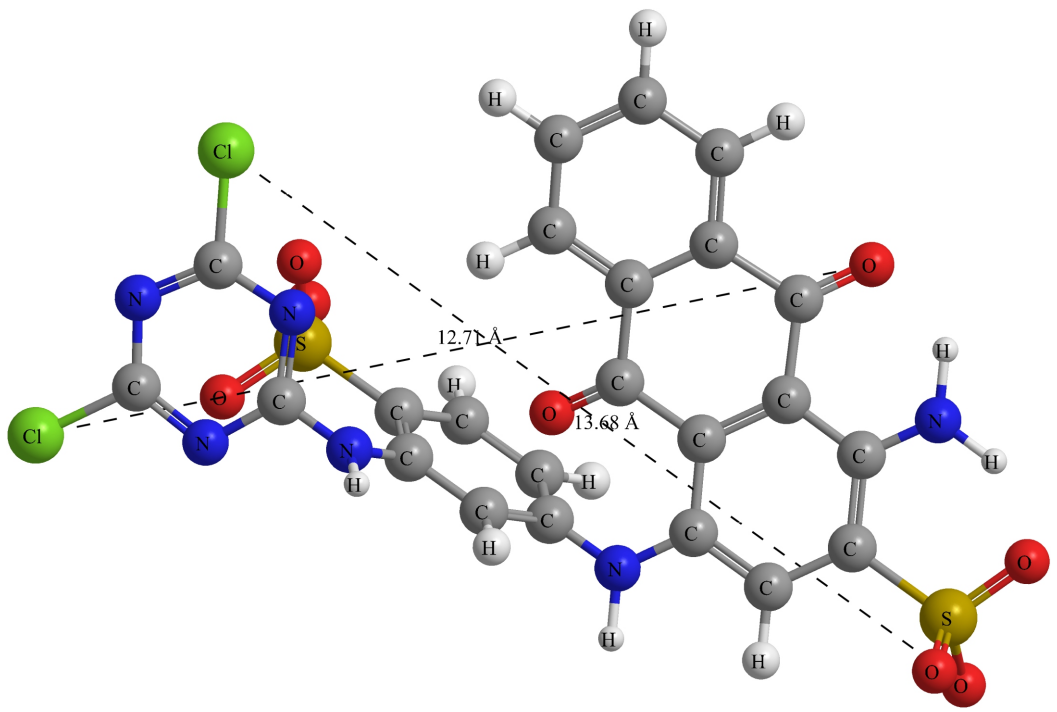

Fig S1- A- Structural Formula of RB-4 dye ($C_{23}H_{12}Cl_2N_6Na_2O_8S_2$) pKa values are indicated in figure; B- optimized three-dimensional structural formula of RB-4 The dimensions of the chemical molecule was calculated using MarvinSketch version 21.1.0. Molecular weight 681.383 g mol^{-1}; Van der Waals volume 454.98 $Å^3$; van der Waals surface area 681.31 $Å^2$ (pH 2.0); Polar surface area 254.05 $Å^2$ (pH 2.0); Dipole Moment 90.94 Debye; Hydrophilic-lipophilic balance 43.50.

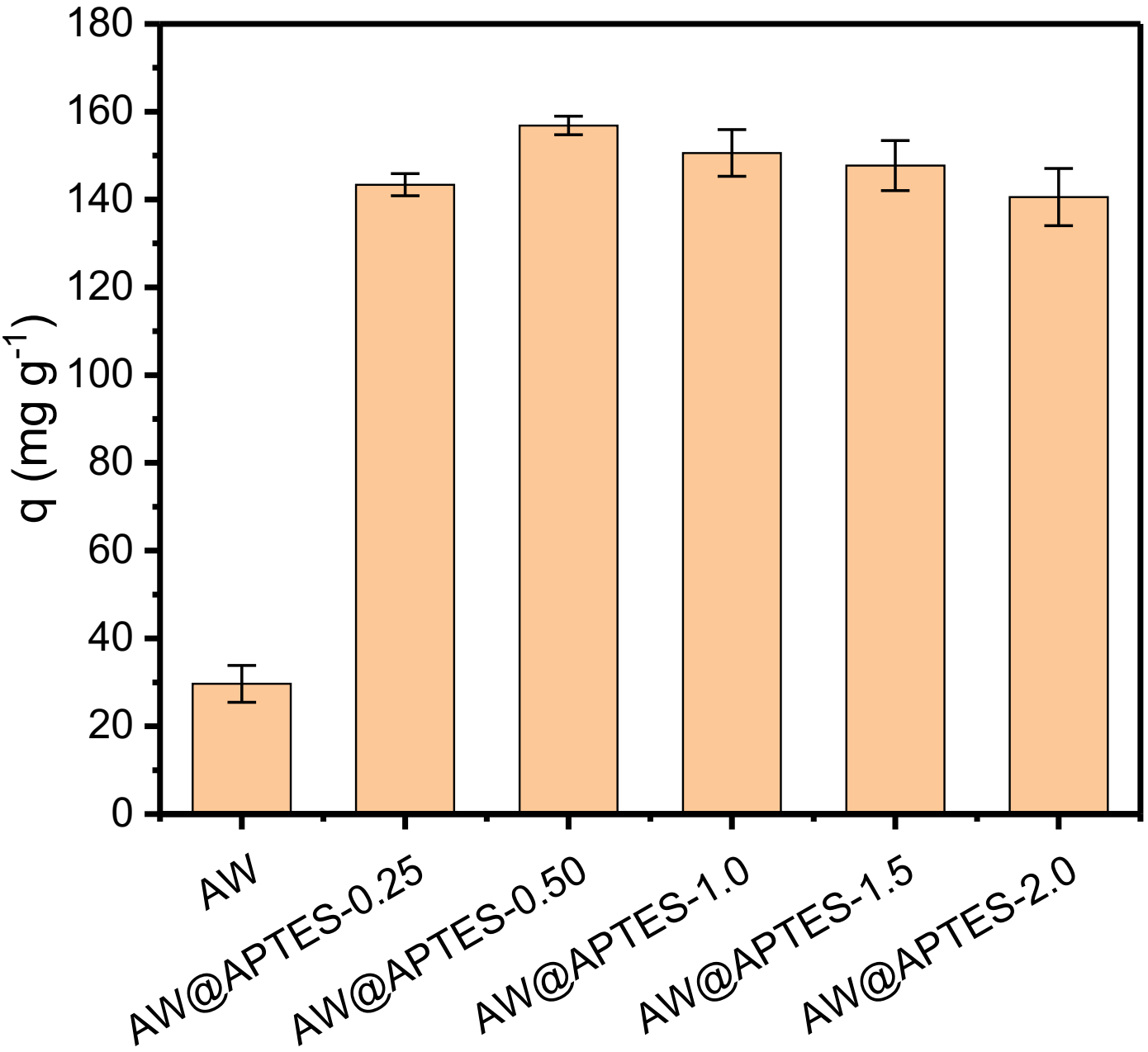

Fig S2. Effect of amount of APTES on the sorption capacity of the adsorbents for removal of 285.0 mg L^{-1} of RB-4 dye. Adsorbent dosage of 1.5 g L^{-1}, initial pH 2, temperature 25°C , time of contact 360 min.

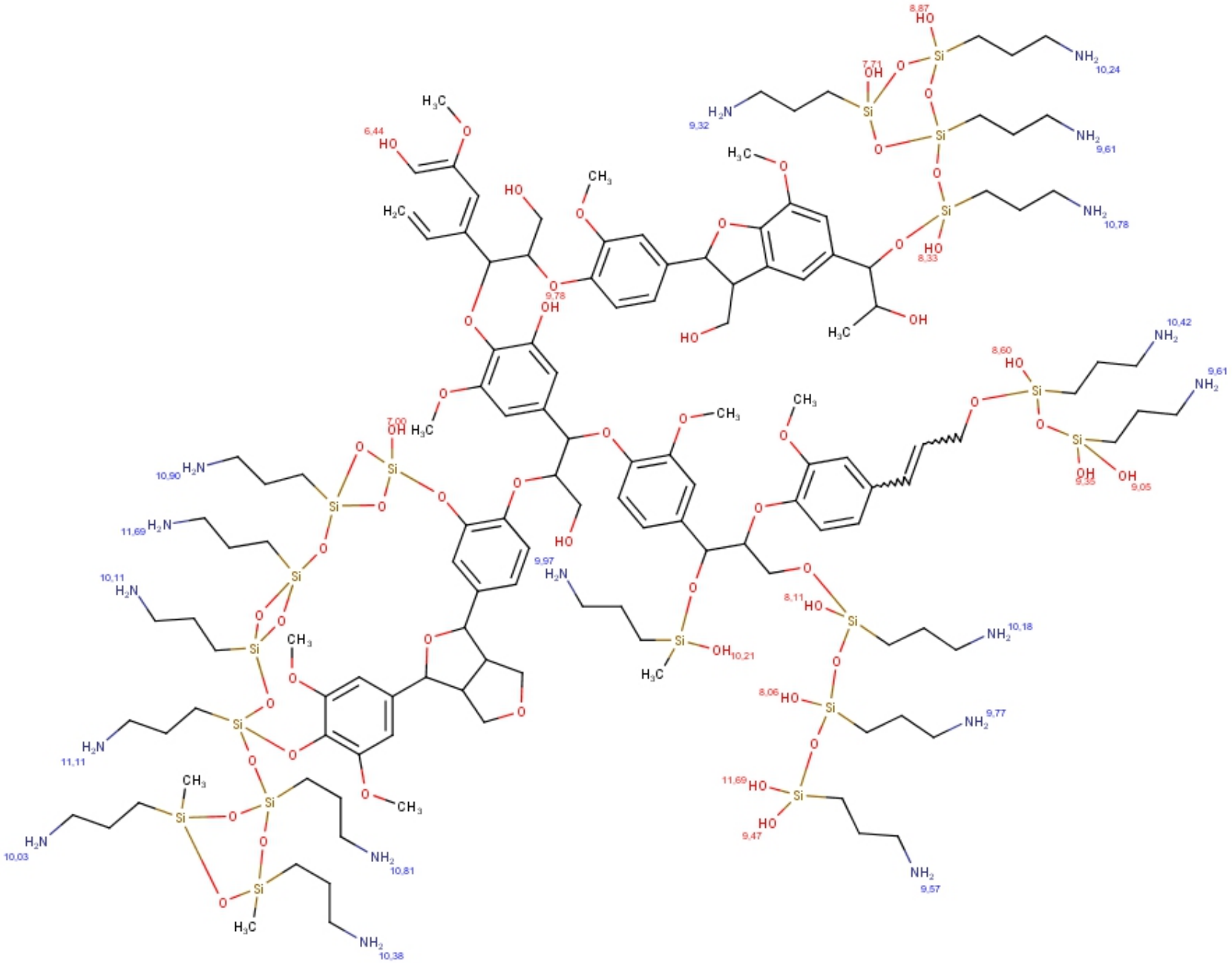

Fig S3. Estimation of values of pK_a for the amino and silanol groups of AW@APTES-0.5

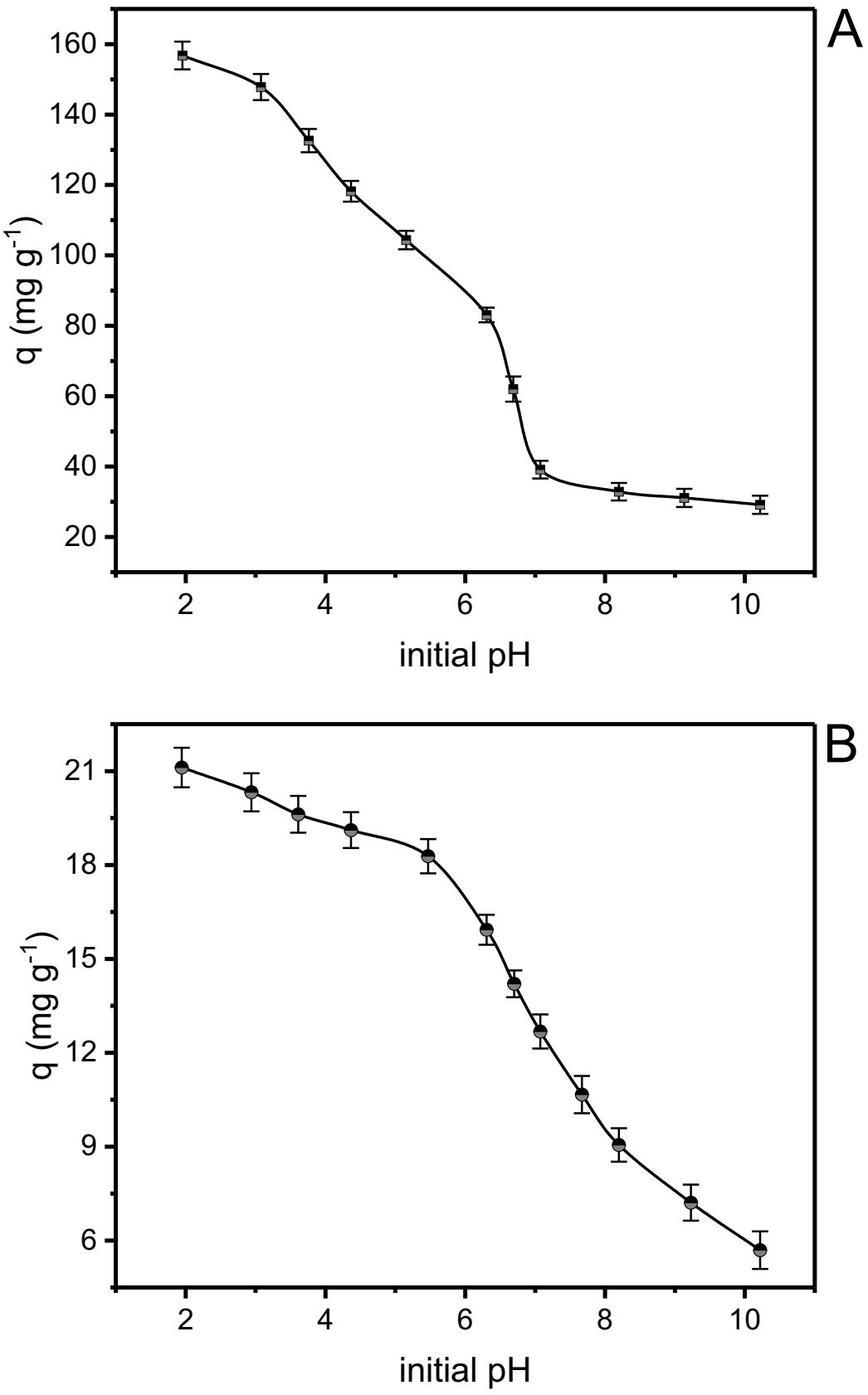

Fig S4. Effect of initial pH on the sorption capacity of A- AW@APTES-0.5; B- AW. Conditions, adsorbent dosage 1.5 g L^{-1}, initial RB-4 300 mg L^{-1}, 25°C, contact time 360 min.

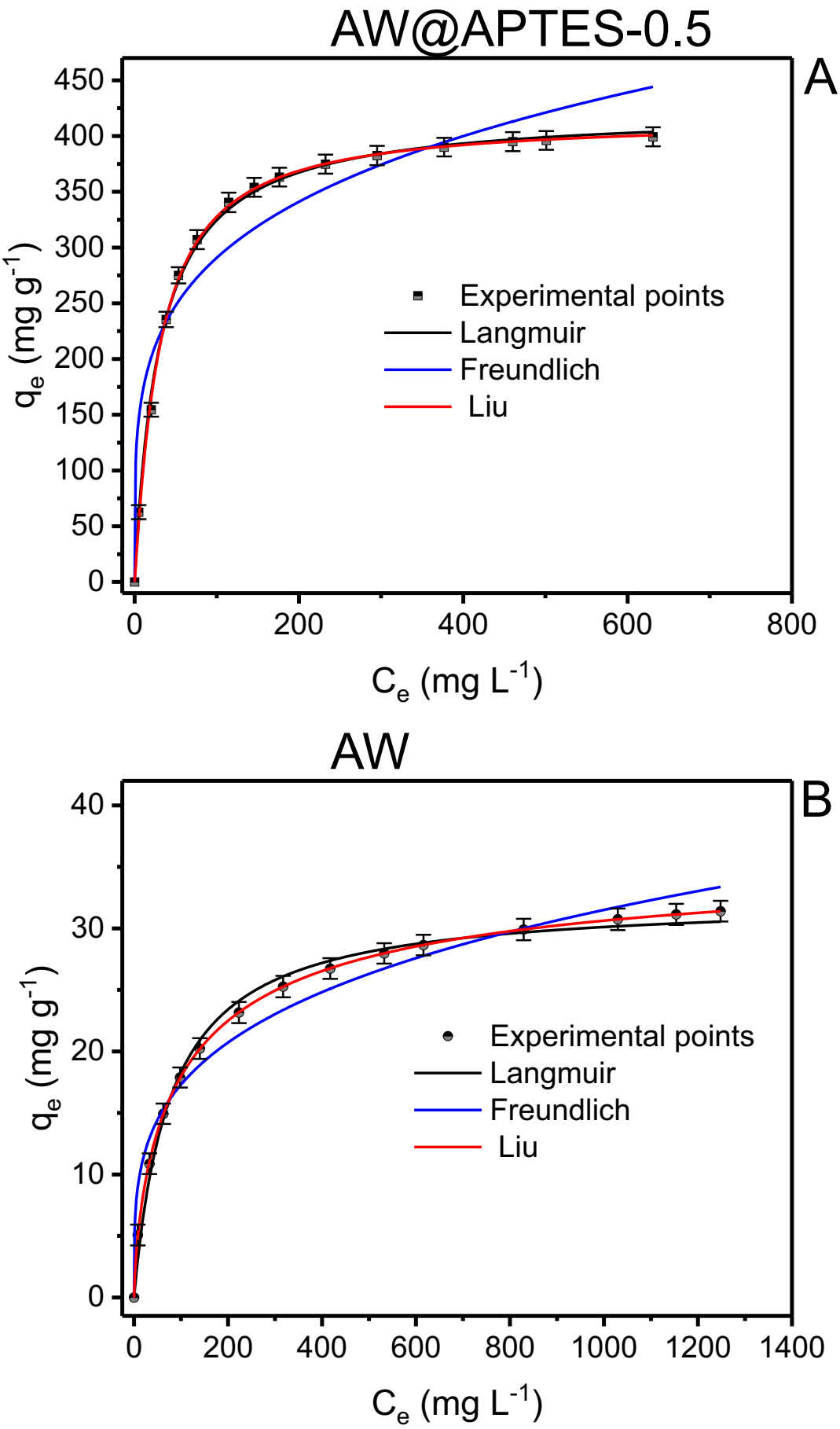

Fig S5. Isotherms of adsorption of RB-4 dye onto, A- AW@APTES-0.5 and B- AW. Conditions initial pH 2.0, adsorbent dosage 1.5 g L^{-1}, T 50°C, time of contact 240 min.

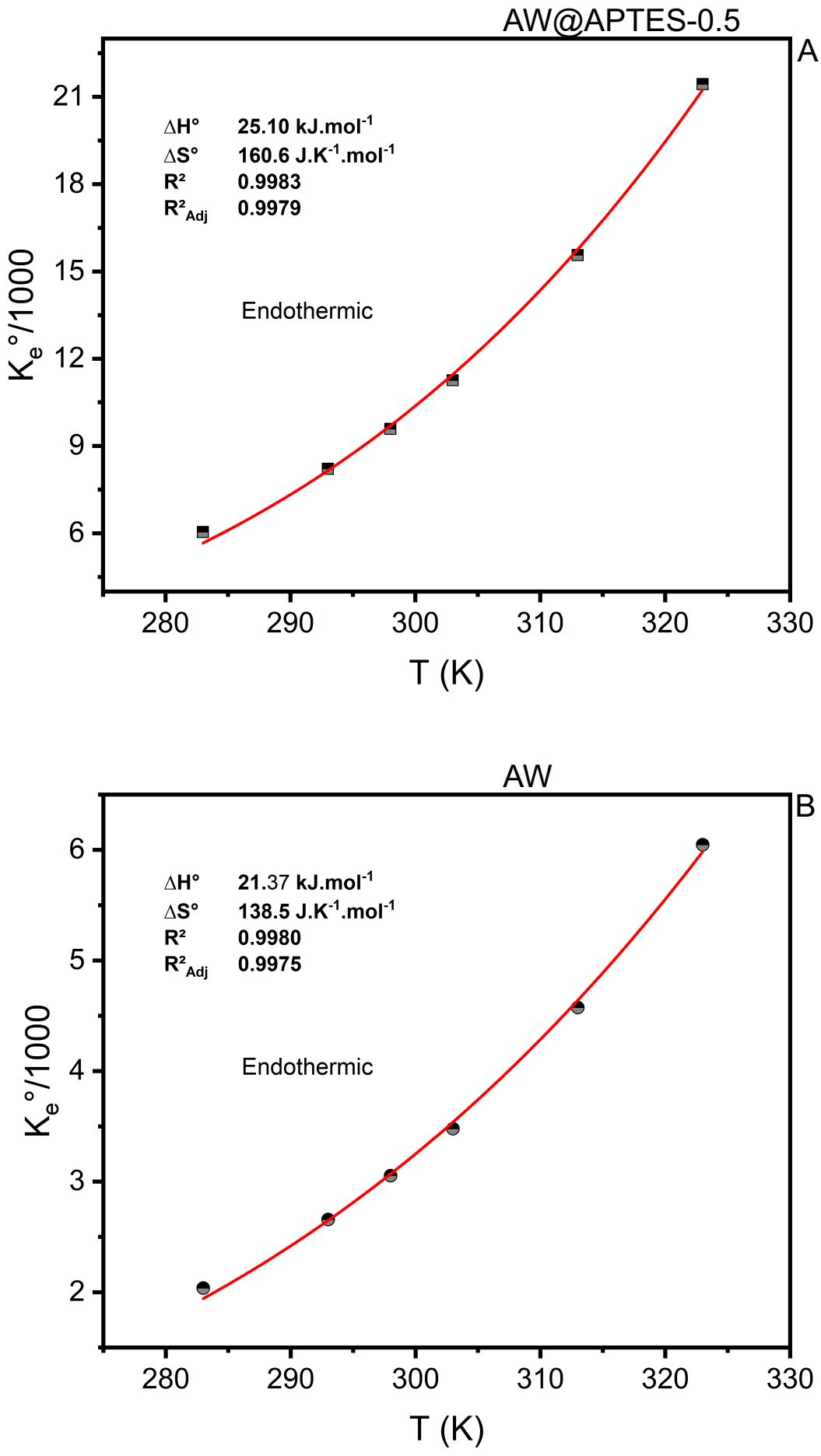

Fig S6. Variation of K adsorpiton equilibrium in function of the temperature. Adsorbate: RB-4 dye, A- AW@APTES-0.5 and B- AW.
Conditions initial pH 2.0, adsorbent dosage 1.5 g L^{-1}, time of contact 240 min.